

Solution space path planning for supporting en-route air traffic control

Yiyuan Zou*, Wenying Lyu, Clark Borst

Control and Simulation, Faculty of Aerospace Engineering, Delft University of Technology, Delft, The Netherlands

Abstract

As technology advances, many path-planning algorithms have been proposed for Air Traffic Management, yet their operational adoption in tactical control remains limited, revealing a misalignment between algorithmic design priorities and air traffic controllers' needs. This underscores the need for decision-support solutions that are inherently interpretable, computationally efficient, and explicitly designed for human use. Focusing on this design challenge, this study develops a conflict-free path-planning algorithm for en-route Air Traffic Control (ATC) designed to be compatible with two guiding considerations: (1) the interpretability and flexibility offered by solution-space displays, which motivate constructing an algorithm that exposes *all* feasible safe actions and accommodates shifting optimization goals; and (2) the decision logic controllers naturally apply when enforcing operational constraints, such as separation standards, maneuverability limits, waypoint minimization, and routing practicality. Centered on these principles, the algorithm integrates three intent-based conflict detection methods—distance-based, time-interval-based, and zone-based—within a solution-space framework to identify conflict-free paths in computationally efficient ways. Additionally, vertex-based and edge-based search nodes are proposed for solution space path planning (SSPP), resulting in two variants—SSPPV and SSPPE, respectively, which are evaluated in terms of computational speed and solution quality. Empirical results show that SSPPV paired with zone-based conflict detection achieves the best performance, computing paths in 3.69 ms on average in operational-relevant scenarios based on the Delta sector of the Maastricht Upper Area Control Centre (MUAC) using a 5 nmi grid. SSPPV remains approximately 3.77 times faster than SSPPE while offering competitive effectiveness, making it suitable for time-critical tactical operations and interactive 'what-if' probing in real time. An extension to SSPPV and SSPPE further examines the trade-off between delay minimization and aircraft separation requirements, demonstrating their flexibility in revising optimization objectives. The primary contribution of this work lies in complementing existing path-planning research by demonstrating how such algorithms can be more effectively aligned with human use and operational requirements, offering a strong foundation for practical integration into future ATC decision-support systems.

Keywords: Air traffic control, Conflict-free path planning, Solution space, Conflict detection and resolution

*Corresponding author

Email addresses: y.zou@tudelft.nl (Yiyuan Zou), w.lyu-1@tudelft.nl (Wenying Lyu), c.borst@tudelft.nl (Clark Borst)

1. Introduction

In response to the increasing demands for efficiency and safety, various technological initiatives have been developed to facilitate automation within the Air Traffic Management (ATM) community. The long-term vision for air traffic modernization, supported by targeted research initiatives, has been strategically formulated [1]. As outlined in the Digital European Sky vision [2], this modernization follows a phased approach: the first three stages primarily focus on enhancing system support while keeping human operators in control, whereas the final stage aims to enable advanced collaboration between human and machine agents, allowing task delegation to effectively manage higher levels of complexity. At higher levels of automation, system performance becomes increasingly dependent on the underlying algorithms, placing greater emphasis on their ability to generate timely, reliable, and operationally meaningful solutions in ways that humans can understand and trust [3, 4, 5].

Despite significant advancements, past experiences have highlighted the ongoing challenges in balancing technological capabilities with human acceptance [6]. Although many algorithms and tools have been developed to support controller decision-making, only a few have been implemented in real-world operations due to limited acceptance by Air Traffic Controllers (ATCos). This is because such automated systems often lack transparency and interpretability, may not fully capture operational contexts and constraints, and/or are misaligned with ATCos' cognitive processes and operational practices. There is also a general consensus that a trade-off exists between algorithmic interpretability and performance [7, 8], and that improving transparency often incurs additional computational overhead [9, 10], which further complicates the adoption of advanced automation in safety-critical environments such as Air Traffic Control (ATC).

To improve system usability and controller acceptance, significant effort has been devoted over the past decades to developing interfaces that bridge the interactions between humans and machines. This has led to the development of an 'ecological' design framework [11, 12, 13], emphasizing the importance of the work domain as the central element that bounds human and machine actions, which inspired the 'solution space' concept explored in aviation [14]. Previous studies have demonstrated the effectiveness of this concept in supporting human decision-making in ATC [15] and many other domains (see [16] for an overview). At the core of this concept is the visual representation of the action space as geometrically interpretable 'go/no-go' regions bounded by a safe envelope governed by causal (e.g., physical) and intentional (e.g., procedural) constraints. The action space enables controllers to freely select any action while considering their potential consequences. By revealing the system's inner structure and constraints, controllers are empowered to undertake actions themselves, quickly understand the impact of certain actions, shift decision-making strategies, and manage complexity. However, in practice, solution space displays often rely on simplified representations (e.g., a single intermediate waypoint for conflict-free rerouting), which, while improving usability, restrict the solution space and bias the search process toward greedy solutions that may prevent the identification of more optimal solutions.

Given the demonstrated benefits of solution space displays in supporting human decision-making and providing

an interpretable representation of the feasible action space, this paper proposes a new perspective on the *design* of decision-making algorithms inspired by solution space concepts. Our approach centers on structuring the algorithm directly around a human-interpretable solution space, in which the set of all feasible, conflict-free actions is explicitly represented and efficiently explored. This representation enables rapid identification of available solutions by exploiting the geometric structure of go/no-go action spaces, thereby reducing computational latency. In addition, the search process is guided by decision principles that reflect how controllers operationally manage constraints—such as separation assurance, maneuverability limits, and route practicality—ensuring that candidate solutions are not only feasible but also interpretable and operationally compliant. By combining a structured, interpretable solution space representation with controller-aligned decision logic, the proposed approach enables fast and targeted exploration of rich solution sets, improving the ability to identify near-optimal solutions while maintaining real-time computational performance. In other words, the core problem considered in this article is how to balance interpretability, computational efficiency, operational compliance, and solution optimality, which we explore through the lens of different algorithmic structures.

To limit the scope of this research, we focus on en-route air traffic control, where the primary task of ATCos is to guide aircraft from entry points to their corresponding exit points within a sector while avoiding conflicts among them. This is essentially a conflict-free path-planning problem. Accordingly, the proposed decision-making algorithm is termed Solution Space Path Planning (SSPP). Compared to existing studies, the main contributions of this paper can be summarized as follows:

- 1) *Interpretability and operational compliance*: We propose the concept of SSPP, which has the potential to improve operator understanding and acceptance by exploring and generating solutions in human-compatible ways through interpretable ‘white-box’ algorithmic structures [9] and corresponding visual representations provided by solution-space interfaces [17, 18]. SSPP also overcomes the limitations of traditional A*-based algorithms, allowing the generation of straighter paths with fewer turns, which is particularly suitable and practical for aircraft navigation. Compared to previous relevant work in aviation [19, 20, 21], SSPP is capable of finding conflict-free paths with multiple intermediate waypoints while maintaining the paths as straight as possible. Moreover, the solution space concept inherently provides flexibility in incorporating various constraints, enabling algorithm designers to tailor SSPP to meet operational requirements.
- 2) *Computational efficiency*: We develop several advanced techniques to accelerate solution-space generation and exploration, paving the way for ATCo ‘what-if’ probing in real time during sector control. For example, to check whether a certain location is unreachable due to *static* obstacles, we apply the recursive shadowcasting algorithm [22, 23] for computing the *field of view* instead of relying on a traditional line-of-sight approach [24, 25]. To account for turning angle limitations of aircraft, the original shadowcasting algorithm has been adapted by incorporating the angle of view (e.g., $[\theta - 60^\circ, \theta + 60^\circ]$ where θ is the current heading of aircraft). For *dynamic* obstacles, we develop three different *intent-based* conflict detection methods for solution space generation: distance-based, time-interval-based, and zone-based. The integration of zone-based conflict detection with the

shadowcasting allows for the creation of a field of view in the presence of dynamic obstacles (not just static obstacles), offering a novel and efficient approach to conflict-free path planning in dynamic environments. Empirical evaluation shows that the zone-based approach is generally faster than both the distance-based and time-interval-based approaches, particularly when the grid size is small.

- 3) *Solution optimality*: We implement A* search [26], rather than greedy search, and propose vertex-based and edge-based search nodes for path planning, leading to two near-optimal versions of SSPP—SSPPV and SSPPE. SSPPE can achieve a higher success rate than SSPPV in finding (near-)optimal solutions by exploring a larger search space, although this comes at the cost of increased computational time. Since the basic goal of SSPP is to find time-optimal paths with minimal delay, we also explore a potential extension that accounts for aircraft separation requirements to enhance solution robustness (bi-objective conflict-free path planning [27, 28]).

The paper is structured as follows: Section 2 reviews related work, with an emphasis on the application of the solution space concept and existing path-planning algorithms. Section 3 outlines the necessary preliminaries, clarifying the path-planning problem in en-route ATC. Section 4 describes how to generate solution spaces using three conflict detection methods, which lays the foundation for the proposed solution space path planning introduced in Section 5. A case study is presented in Section 6, followed by a discussion of the results in Section 7. Section 8 concludes the article and outline directions for future research.

2. Related work

2.1. Solution space concept

In area control, ATCos are responsible for ensuring the safe and efficient movement of aircraft between sectors. They continuously monitor and manage traffic in real time to prevent conflicts, enforce airspace procedural constraints, and maintain optimal flow. However, increasing traffic volumes and the shift toward advanced operational concepts—such as stepping away from fixed geographical boundaries and moving to time-based trajectory management—have significantly increased the complexity of tactical decision-making. This increasing complexity, coupled with the need for more effective automation support, has driven the development of the solution space concept in decision support tools [17], which have recently reached operational implementation. For example, in 2024, the Maastricht Upper Area Control Centre (MUAC) developed and implemented the Lateral Obstacle & Resolution Display (LORD) for conflict resolution support [29].

The solution space refers to the set of feasible actions that ensure safety while meeting operational constraints. Instead of directly presenting solutions, the portrayed envelope highlights the constraints that define these feasible actions, allowing controllers to ‘see’ the available options and make their own decisions within the boundaries set by these constraints. Building on this concept, various tools have been developed for supporting humans in performing ATC tasks (e.g., conflict detection and resolution) [30], such as the Highly Interactive Problem Solver (HIPS), the Solution Space Diagram (SSD), and the Travel Space Representation (TSR). The SSD, based on velocity obsta-

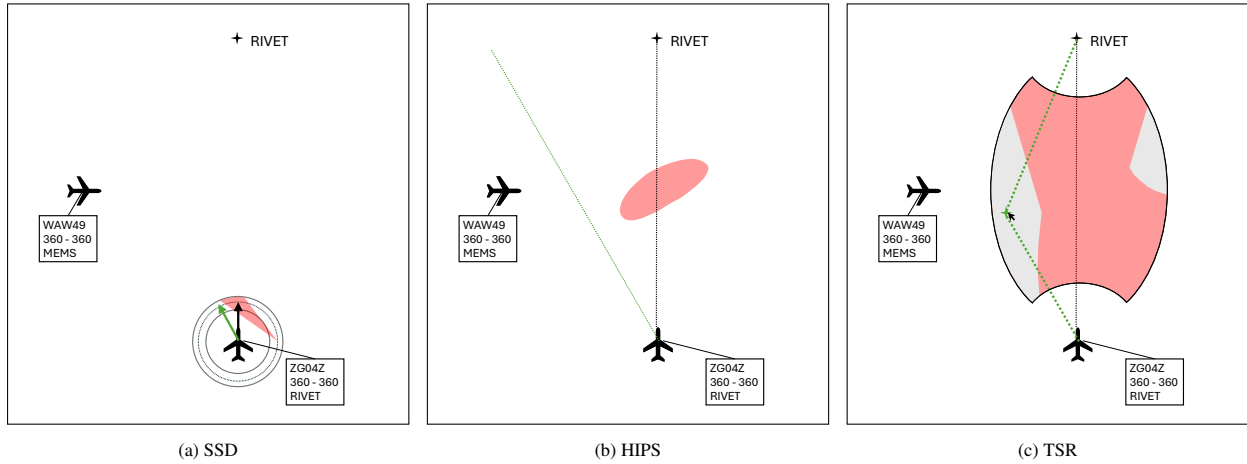


Figure 1: Comparison of SSD, HIPS, and TSR representations.

cles [31, 32, 33], portrays heading and speed constraints around the velocity vector of the selected aircraft and within the minimum and maximum speed envelope [34, 35, 36]—a concept that also underlies MUAC’s LORD system [29]. HIPS shows geographical locations of conflict zones along the planned trajectory, distinguishing between safe and unsafe paths by trajectory extrapolation [37, 15]. TSR portrays conflict-free regions for placing intermediate waypoints within an envelope of allowable time delays, particularly for rerouting tasks that empower the controller to manipulate flight trajectories while adhering to spatial-temporal constraints [38, 39, 40].

As shown in Figure 1, when a controlled aircraft is approaching a target waypoint but is at risk of conflict with an intruder aircraft, SSD, HIPS, and TSR each provide different visualizations of the situation. Both SSD and HIPS highlight conflict zones in red—SSD with respect to the velocity vector, and HIPS along the absolute trackline. For both the SSD and HIPS, the ATCo can resolve the conflict by changing the aircraft’s heading and/or speed. TSR similarly highlights unsafe regions in red, but these regions now indicate the set of unsafe intermediate waypoints. The key distinction lies in how TSR represents conflict-free options: it considers a series of potential rerouting segments that temporarily deviate from the original flight path to bypass the conflict before returning to the planned route. This enables controllers to perceive safe intermediate waypoint choices, supporting both conflict resolution and rerouting tasks. The TSR is primarily designed for scenarios that involve rerouting via a *single* intermediate waypoint, a simplification that enhances usability and interpretability. ATCos are free to select any point within the safe zone, with the main trade-off being additional track miles and potential time delays.

Empirical studies have demonstrated that these tools are effective in supporting ATCos, largely due to their high interpretability and intuitive visual representations [14, 36, 17, 41]. However, they do not necessarily lead to improved operational efficiency and often fail to yield optimal solutions. For example, when using TSR, only a single intermediate rerouting waypoint is allowed for each planning session, which may be inefficient when multiple intruder aircraft are present. Consequently, another line of research has emerged, focusing on the development of advanced automation, such as conflict-free path-planning algorithms, for supporting optimal control and decision-making.

However, this increasing level of automation often comes at the cost of reduced interpretability and transparency, making such algorithms more difficult for human operators to understand and trust [42, 9]. This limitation significantly hinders their operational applicability, particularly in safety-critical domains such as ATC. This trade-off between performance optimization and user acceptance remains a central challenge in the design of decision-support systems [6]. Therefore, building on the foundation of interpretable solution space interfaces—which have found their way into operational use and gained broad acceptance—this paper introduces a novel Solution Space Path Planning (SSPP) algorithm. The approach aims to achieve (near-)optimal routing at low computational speeds while preserving the structural properties that support ATCo interpretability, although interpretability itself is not explicitly evaluated through a user study in this article. Before delving into the details of SSPP, the next section first provides an overview of related work on existing path-planning algorithms and highlights the contributions of our proposed approach.

2.2. Path planning algorithms

A* [26] is one of the most well-known path-planning algorithms, which can find optimal paths within predefined graphs efficiently, like regular grids, visibility graphs and navigation meshes [43, 44]. It has been applied for fixed-wing aircraft path planning [45]. However, the paths found by traditional A* are highly affected by the graph shape. In regular square grids, the turning angles of A* paths are limited to 45-degree increments, such as 45°, 90°, and 135°, due to its 8 adjacent neighbors. This may lead to an excessive number of turning points and overly large turning angles in paths, making the traditional A* unsuitable for crewed aircraft. Some research attempted post-hoc smoothing to straighten the final paths [46], but this approach may not always be effective when multiple constraints are present.

To address this issue, any-angle path planning was proposed [24, 47, 48, 49], which ignores the edges of predefined graphs and allows any-angle turns at the vertices. Instead of performing post-hoc smoothing, any-angle path planning searches for smooth paths directly during the planning process. Some techniques have been developed for any-angle path planning. For example, rather than 8 neighbors, one can use extended 2^k ($k > 3$) neighbors for node expansion [49]. In this way, the A* search can skip the adjacent grid cells to find straighter paths. Alternatively, one can examine whether a newly expanded node can be reached by the parent of the current node, like Theta* [24]. Any-angle path planning has been applied for fixed-wing aircraft as well [50].

Nonetheless, the aforementioned algorithms are only applicable to static obstacles. They cannot avoid conflicts between aircraft. For conflict-free path planning, the simplest approach may be to utilize TSR. Since TSR evaluates all potential rerouting points, such as each cell in a grid, one can directly choose the point with the lowest cost (e.g., minimum delay) [20]. However, this approach is limited to finding paths with a single turning point, making it less effective in complex scenarios. To relax this restriction, A* can be adapted to consider dynamic obstacles as well. A common approach is to divide the time dimension into multiple equal-length time slots, creating a space-time grid [51, 19, 21]. Dynamic obstacles can thus be mapped onto this space-time grid and converted into static obstacle cells. Then, A* can be used to find conflict-free paths within this space-time grid. However, this method introduces a new dimension to the search space, which aggravates the *curse of dimensionality* problem [52] (i.e., the algorithm speed

may drop significantly as the dimension increases). To address this issue, Safe Interval Path Planning (SIPP) [53] was proposed. Rather than using a space-time grid, SIPP computes safe intervals for each cell, indicating periods during which the cell is unoccupied by obstacles and thus safe for path planning. It avoids discretizing the time dimension and can generate a *compact* space-time search space. SIPP has been applied for aircraft taxiing operations [54].

However, SIPP faces similar problems as A*. The turning angles of SIPP paths are also limited to 45-degree increments. Therefore, combining both SIPP and any-angle path planning, Any-Angle SIPP (AA-SIPP) was developed [55]. Similar to Theta*, AA-SIPP checks whether the parent of the current node can reach a newly expanded node at a lower cost. This smoothing takes dynamic obstacles into account as well. However, also like Theta*, AA-SIPP cannot guarantee finding optimal paths. Time-Optimal AA-SIPP (TO-AA-SIPP) [25] was thus proposed. Instead of merely straightening the path locally around the current node, TO-AA-SIPP examines the entire search space and globally constructs paths that are as straight as possible. This operation could be highly time-consuming [25, 56].

To speed up TO-AA-SIPP, Zeta*-SIPP [56] was developed. In Zeta*-SIPP, a new type of forward expansion tailored for optimal any-angle path planning was introduced: *elliptical forward expansion*. Elliptical forward expansion does not proceed in a grid-by-grid or 2^k -grid manner; instead, it expands nodes following an elliptical pattern. By leveraging the properties of ellipses, it can be proven that this elliptical expansion is sufficient for optimal any-angle path planning. Another technique introduced in Zeta*-SIPP is the *field of view*. It is a more efficient approach than the line of sight for detecting conflicts with static obstacles and building visibility connections between nodes.

The SIPP-based algorithms mentioned above are all single-agent methods, which can serve as low-level planners for multi-agent path planning [55, 57, 58]. The first-come-first-served strategy [20], commonly used in aviation, is well-suited for Priority-Based Search (PBS) [54, 55]. This means that aircraft already within the sector are considered dynamic obstacles for newly incoming aircraft. In this study, we also implement this strategy. Optimal multi-agent pathfinding methods, such as Conflict-Based Search (CBS) [59], Continuous-time CBS (CCBS) [57], and Any-Angle CCBS (AA-CCBS) [58], are beyond the scope of this article.

In addition to the search-based algorithms discussed above, there is a rapidly growing interest in machine learning-based methods [60, 61]. However, in aviation, such methods still face significant challenges regarding their trustworthiness and certification [62]. Their inherent “black-box” nature may hinder acceptance and trust from ATCos. Some efforts have been made to mitigate this issue through Explainable AI (XAI) and increased transparency [42]. For example, Herman [63] employed an explainable reinforcement learning technique [64] that decomposes the overall reward into multiple meaningful components, thereby revealing the underlying rationale behind each maneuvering behavior. Papadopoulos et al. [65] introduced the concept of operational transparency, which aims to reveal relevant operational information to help ATCos maintain situation awareness and intervene in a timely manner. Zou and Borst [4, 66] proposed a unified transparency taxonomy to integrate operational and engineering transparency, although they focused on search-based algorithms rather than learning-based approaches.

Despite these ongoing efforts, there is still a long way to go before machine learning-based methods can be applied in operational ATC environments. Therefore, this study centers on search-based path planning, considering its solid

mathematical foundations, theoretical optimality guarantees and inherent interpretability. These characteristics make search-based methods more reliable and suitable for real-world deployment.

The core of conflict-free path planning is conflict detection. In aviation, the Closest Point of Approach (CPA) is the most commonly used metric, whereas safe intervals are mainly employed in SIPP-based path planning. Therefore, we integrate distance-based (CPA) and time-interval-based (SIPP) conflict detection methods into SSPP for comparison. Inspired by HIPS, we also propose a novel conflict detection method for path planning based on conflict zones (zone-based conflict detection). This method inherits the good interpretability of HIPS and is fully compatible with the field of view. Moreover, we develop two versions of SSPP and introduce a new objective function for the trade-off between delay and separation.

Comparing to existing path-planning algorithms, the proposed SSPP is similar to the naive TO-AA-SIPP [25]. At each step, SSPP generates a solution space to indicate which nodes are reachable from the current node. However, unlike TO-AA-SIPP, the solution space in SSPP incorporates real-world constraints, and the field of view is leveraged to facilitate its generation. Another closely related study is conducted by Chen et al. [20], which similarly proposes a path-planning algorithm for en-route airspace operations and employs the solution space concept to support controller decision-making. In their approach, *distance-based conflict detection* is used to construct the solution space, while the search space is restricted to a *single* intermediate rerouting point. Under this formulation, SSPP-D (where D denotes distance-based conflict detection) with only one rerouting point can be viewed as a variant of their algorithm.

3. Preliminaries

In this section, we clarify the path-planning problem in en-route ATC. To simplify the problem, we make the following assumptions:

- 1) *Consider only 2D instead of 3D.* As the airspace is divided into multiple flight levels, it is reasonable to focus only on 2D within each flight level.
- 2) *The aircraft speed remains constant.* This is a common assumption in the path-planning field, and altering aircraft speed in en-route phases is generally not part of ATCos' decision-making practice.
- 3) *Ignore aircraft turning dynamics and trajectory uncertainties.* Turning dynamics and trajectory uncertainties significantly complicate the problem. Rather than attempting to model these uncertainties explicitly, we follow established ATC practice: ATCos typically address such uncertainties by applying additional separation buffers, which can likewise be incorporated into the minimum safe separation constraint (i.e., 5 nmi).

Therefore, path planning for en-route aircraft is a problem of determining a path from a start point p_s to a target point p_t given a 2D space $S \subset \mathbb{R}^2: (p_s, p_t, S)$. Static obstacles (for example, prohibited airspace, military zones, etc.) are defined as $O = O_1 \cup O_2 \cup \dots \cup O_n \subset \mathbb{R}^2$. To further limit the complexity of the problem, we discretize the free space $S_{free} = S \setminus O$ using a grid $G = (V, E)$ where V is a set of vertices, $E \subseteq V \times V$ is a set of edges. Then, the 2D path-planning problem can be rewritten as (p_s, p_t, G) .

A *path* is a sequence of points $\pi = \{p_1, p_2, \dots, p_n\} \subset G$ where $p_1 = p_s$ and $p_n = p_t$. The *cost* of a path π is the sum of the flight duration between each successive pair of points: $C(\pi) = \sum_{i=1}^{n-1} \text{dist}(i, i+1) / \|\mathbf{v}\|$ where $\text{dist}(i, i+1)$ is the distance between the points p_i and p_{i+1} and $\|\mathbf{v}\|$ is the aircraft speed. We assume that the paths of other aircraft (dynamic obstacles) are known: $\{\pi^1, \pi^2, \dots, \pi^k\}$. Thus, the goal of the path planning is to find the time-optimal path between p_s and p_t without conflicts with other aircraft.

In path planning, the total cost of a node is $f(n) = g(n_s, n) + h(n, n_t)$. $g(n_s, n)$ denotes the real cost (flight duration) from the start node n_s to the node n and is initially set to infinity. If $g(n_s, n)$ is less than infinity, it means that a feasible path to the node n has been found. $g(n, n')$ is the real cost from the node n to another node n' . $h(n, n_t)$ refers to the estimated cost from the node n to the target node n_t , which we assume to be the flight duration of the direct path between n and n_t . $h(n, n')$ is the estimated cost from n to n' . In the path-planning field, $g(n_s, n)$ is usually written as $g(n)$, while $h(n, n_t)$ is commonly simplified to $h(n)$.

For en-route aircraft path planning, several procedural constraints should be considered:

- 1) *Minimum separation standards.* En-route aircraft should maintain a horizontal separation of over 5 nmi or a vertical separation of at least 1000 ft. In this research, we only consider horizontal separation.
- 2) *Maximum allowable time delay.* A Required Time of Arrival (RTA) is usually defined to ensure the efficiency of trajectory-based operations. The maximum allowable time delay indicates the RTA tolerance, meaning that the candidate paths leading to excessive delays should be discarded.
- 3) *Turning angle limitation.* Aircraft are unable to make sharp turns due to their maneuverability limitations and passenger comfort, which means that the angle between two path segments should be limited.
- 4) *Minimum distance between waypoints.* The distance between two waypoints should not be excessively short; otherwise, aircraft may be unable to execute turns and might deviate significantly from the intended trajectory.
- 5) *Maximum number of rerouting waypoints.* ATCos may wish to limit the number of rerouting points for aircraft. This constraint enables ATCos to customize the algorithm to align with their preferences.

4. Solution space generation

To tackle the path-planning problem described above, we develop a novel algorithm named Solution Space Path Planning (SSPP). Basically, SSPP generates a solution space for the next point from the current point at each step, executing A* search [26] to continuously explore the space until the target point is reached. The core of SSPP lies in generating a solution space to identify all reachable points from a given location, which resembles ideas like reachable sets [67]. However, in SSPP, we integrate several techniques to accelerate the process of solution space generation, including three different conflict detection methods. Combining solution space with search-based path planning also allows us to readily visualize the internal process of SSPP for supporting ATCo supervision [9].

Algorithm 1 depicts the solution space generation during the search process, including the constraints outlined in Section 3. The `generateSearchRegion` creates an elliptical boundary according to the current and target nodes and

Algorithm 1 Solution Space Generation

Require: start node n_s , target node n_t , current node n , current heading θ , maximum allowable delay T_d , maximum turning angle θ_0 , minimum distance between waypoints d_{near}

- 1: **function** generateSolutionSpace(n, θ)
- 2: solution space $S \leftarrow \emptyset$
- 3: remaining time $T \leftarrow h(n_s) + T_d - g(n)$
- 4: $N_{ellipse} \leftarrow \text{generateSearchRegion}(n, n_t, T)$
- 5: $N_{circle} \leftarrow \text{generateNearDistRegion}(n, d_{near})$
- 6: $AOV \leftarrow [\theta - \theta_0, \theta + \theta_0]$
- 7: $N_{visible} \leftarrow \text{shadowcasting}(n, AOV)$
- 8: **for each** node $n' \in N_{visible} \cap N_{ellipse} \setminus N_{circle}$ **do**
- 9: **if** conflictDetection(n, n') = *false* **then**
- 10: $S \leftarrow S \cup \{n'\}$
- 11: **end if**
- 12: **end for**
- 13: **return** S
- 14: **end function**

the remaining flight time T . The nodes outside the elliptical boundary are deemed unreachable from the current node due to the maximum allowable time delay constraint. The `generateNearDistRegion` reflects the minimum distance constraint between waypoints, and the nodes inside the circle N_{circle} should be discarded. Line 6 converts the turning angle constraint into the Angle of View (AOV). Combined with AOV, Line 7 applies recursive shadowcasting [22, 23] to find the nodes visible from the current node. More details of the shadowcasting are presented in Section 4.1. The `conflictDetection` in Line 9 is to detect whether the path segment $[n, n']$ would encounter any conflict with other aircraft. In summary, the `shadowcasting` prevents collisions with static obstacles whereas the `conflictDetection` detects conflicts with dynamic obstacles. The conflict detection methods are discussed in Section 4.2.

4.1. Visibility checks

Before illustrating the shadowcasting algorithm, we first introduce the concept of visibility checks. If two points are mutually visible, the path connecting them will be free from collisions with static obstacles. The line of sight is a common approach to execute such visibility checks on grids for path planning [24]. Specifically, one can apply a line drawing algorithm [68, 69] to find the cells occupied by a path segment and then examine whether any occupied cell is an obstacle. Once the line of sight is blocked, the two points are considered mutually invisible. The occupancy check can be integrated into the line drawing algorithm for early termination of computations. However, the line of sight may be inefficient to compute visibility between the current node and its reachable nodes in the solution space generation because the nodes proximate to the current node would be repeatedly examined. Additionally, the nodes within the shadow of obstacles are unnecessary to be considered, but the line of sight does not take this into account. Therefore, instead of the line of sight, the field of view is implemented to improve the performance of visibility checks, like shadowcasting [22, 23].

The shadowcasting algorithm divides the grid into eight octants. Using a linear transformation, the slope range of

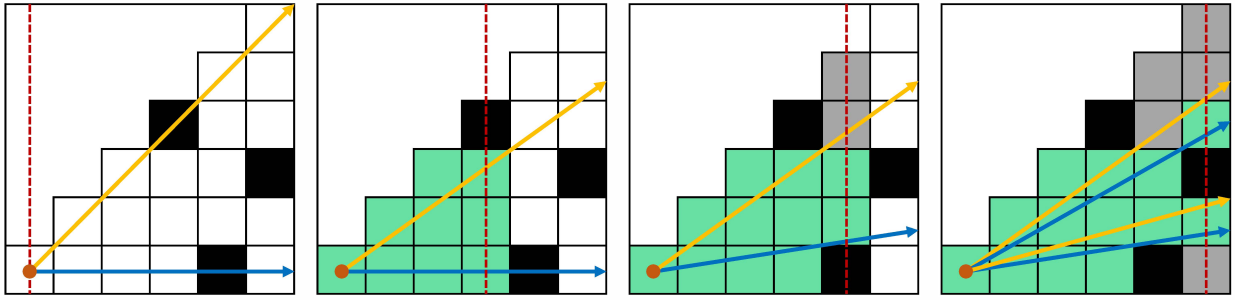


Figure 2: Symmetric recursive shadowcasting, adapted from [23].

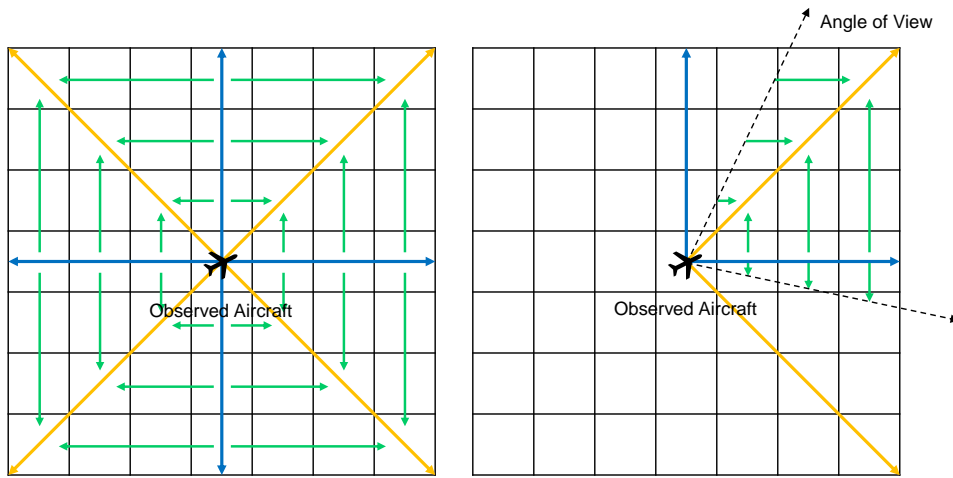


Figure 3: Shadowcasting with Angle of View (AOV).

each octant can be all converted into $[0, 1]$ (i.e., $[0^\circ, 45^\circ]$). As depicted in Figure 2, the algorithm iterates column by column from the origin (red dot). The red dashed line represents the column currently being scanned, while the green cells denote the cells that have been identified as visible from the origin. At each column, the scan direction is from the blue line to the orange line. When it encounters a blocked cell (black), the scan range shrinks for the subsequent columns. Sometimes, it may yield multiple scan ranges after a few columns because of an obstacle in the middle. The blocked cells cast shadows (gray) that are invisible from the origin. The algorithm ensures that each cell is examined only once to construct the field of view. Given that the nodes are positioned at the centers of the grid cells, the cells are visible only when their centers fall within the scan range. This is also called symmetric recursive shadowcasting. Since the start point of an aircraft may not be located at a grid center, we adapt the algorithm to function even in such cases. To incorporate the turning angle constraint into the shadowcasting, we also integrate the AOV and limit the scan range accordingly, as shown in Figure 3. The scan ranges for the octants within the AOV would be recalculated, while those outside would not be scanned.

Algorithm 2 Conflict detection based on separation distance

```
1: function distConflictDetection( $n, n'$ )
2:    $l \leftarrow [n, n']$ 
3:   duration  $T_l \leftarrow [g(n), g(n) + g(n, n')]$ 
4:   for each other aircraft  $m$  do
5:     path segments  $L_m \leftarrow \text{filterPathSegment}(L_m, T_l)$ 
6:     for each path segment  $l_m \in L_m$  do
7:        $d_{min} \leftarrow \text{computeMinSeparation}(l, l_m)$ 
8:       if  $d_{min} < 5$  nmi then
9:         return true
10:      end if
11:    end for
12:  end for
13:  return false
14: end function
```

4.2. Conflict detection

Conflict detection lies at the heart of solution space generation and its performance can significantly influence the computational efficiency of the process. This section presents three distinct conflict detection methods embedded in the solution space generation.

4.2.1. Conflict detection based on separation distance

The first method is conflict detection based on separation distance. A conflict is detected if the predicted minimum separation between aircraft is less than the minimum separation standard (i.e., 5 nmi). The procedure of this method is depicted in Algorithm 2. Line 5 indicates that only path segments within T_l are considered. To compute the predicted minimum separation between l and l_m in Line 7, we first need to cut l to make its start time align with l_m . Then, we can regard l and l_m as rays extending from their respective start points (from time 0). The predicted time to the Closest Point of Approach (CPA) t_{cpa} and the predicted separation at CPA $\|\Delta\mathbf{p}(t_{cpa})\|$ can be computed by [70]

$$t_{cpa} = -\frac{\Delta\mathbf{v}^T \Delta\mathbf{p}(0)}{\|\Delta\mathbf{v}\|^2} \quad (1)$$

$$\|\Delta\mathbf{p}(t_{cpa})\| = \frac{\|\Delta\mathbf{v} \times \Delta\mathbf{p}(0)\|}{\|\Delta\mathbf{v}\|} \quad (2)$$

where $\Delta\mathbf{v}$ is the relative velocity and $\Delta\mathbf{p}(t)$ is the relative position at time t . If $\|\Delta\mathbf{v}\| = 0$, t_{cpa} is defined as 0. Hence, the predicted minimum separation for two rays is

$$\|\Delta\mathbf{p}\|_{min} = \begin{cases} \|\Delta\mathbf{p}(t_{cpa})\| & t_{cpa} > 0 \\ \|\Delta\mathbf{p}(0)\| & t_{cpa} \leq 0 \end{cases} \quad (3)$$

However, l and l_m are not real rays, and the flight duration of each path segment should be considered as well. Let

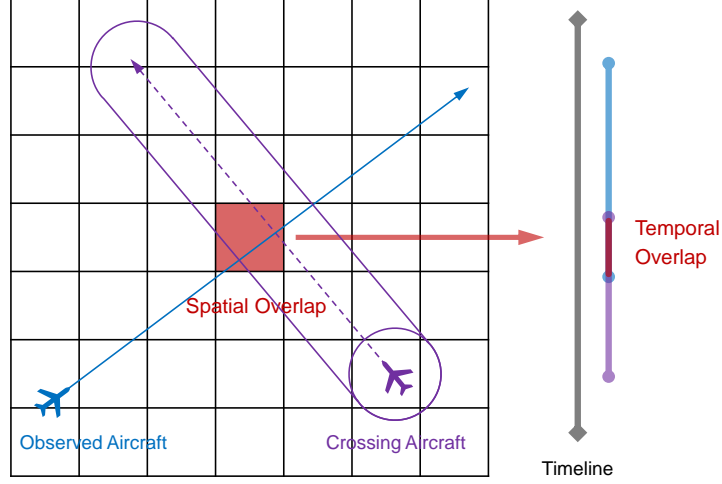


Figure 4: Conflict detection based on time intervals.

t_l be the flight duration of l and $t_{l,m}$ denote the flight duration of l_m . Then, $t_{min} = \min\{t_l, t_{l,m}, t_{cpa}\}$ and the predicted minimum separation for the path segments is

$$\|\Delta\mathbf{p}\|_{min} = \begin{cases} \|\Delta\mathbf{p}(t_{min})\| & t_{min} > 0 \\ \|\Delta\mathbf{p}(0)\| & t_{min} \leq 0 \end{cases} \quad (4)$$

The Equation 4 can be applied to computeMinSeparation in Algorithm 2.

4.2.2. Conflict detection based on time intervals

The second conflict detection method is known as grid-based or time-interval-based conflict detection [71, 72]. It has been widely applied in the path-planning field, such as Safe Interval Path Planning (SIPP) [53]. The distance-based conflict detection checks whether the distance between aircraft is less than the minimum separation standard within the same period, whereas the time-interval-based approach examines whether the time intervals occupied by aircraft overlap within the same area. As illustrated in Figure 4, the crossing aircraft is a dynamic obstacle for the observed aircraft, and a conflict arises if there is a temporal overlap between these two aircraft at the intersecting grid cells. The time-interval-based approach eliminates the need to discretize the time dimension into multiple equal-length time slots, resulting in a compact space-time map that effectively reduces the search space.

The details of this method are presented in Algorithm 3 where C denotes the occupied grid cells and I represents their corresponding occupied time intervals. Lines 6-8 means that if the mapToGrid operation for the path segment l_m has not yet been performed, it will be executed and the results will be stored in $C_{l,m}$ and $I_{l,m}$. This ensures that the mapping will not be repeated in subsequent iterations, thereby conserving computing resources. Line 9 indicates a spatial overlap, and then if any temporal overlap is observed, as depicted in Line 11, a conflict exists.

Algorithm 3 Conflict detection based on time intervals

```
1: function timeConflictDetection( $n, n'$ )
2:    $l \leftarrow [n, n']$ 
3:   cells and intervals  $C_l, I_l \leftarrow \text{mapToGrid}(l, \text{Grid})$ 
4:   for each other aircraft  $m$  do
5:     for each path segment  $l_m$  do
6:       if  $C_{l,m} = \emptyset$  then
7:          $C_{l,m}, I_{l,m} \leftarrow \text{mapToGrid}(l_m, \text{Grid})$ 
8:       end if
9:        $C_{\text{intersect}} \leftarrow C_l \cap C_{l,m}$ 
10:      for each cell  $c \in C_{\text{intersect}}$  do
11:        if  $I_l(c) \cap I_{l,m}(c) \neq \emptyset$  then
12:          return true
13:        end if
14:      end for
15:    end for
16:  end for
17:  return false
18: end function

19: function mapToGrid( $l, \text{Grid}$ )
20:   cells  $C_l \leftarrow \text{intersectGrid}(l, \text{Grid})$  and  $I_l \leftarrow \emptyset$ 
21:   for each cell  $c \in C_l$  do
22:     intervals  $I_l(c) \leftarrow \text{computeTimeInterval}(l, c)$ 
23:   end for
24:   return  $C_l, I_l$ 
25: end function
```

The `mapToGrid` is fundamental to the time-interval-based conflict detection method. For the observed aircraft, a line drawing algorithm [68, 69] can be adapted to identify occupied cells and compute time intervals. However, for the crossing aircraft (dynamic obstacle), a circle indicating the minimum separation also needs to be considered. As shown in Figure 5, we first identify the grid cells occupied by the circle moving along the aircraft trajectory. To precisely calculate the occupied time intervals, it is necessary to find the moments when the moving circle hits and leaves the borders of grid cells. Since grid cells are regular squares, we only need to pay attention to the grid vertices and tangent points (red dots). The entry and exit times for each vertex and the contact time for each tangent point can be calculated. Therefore, the occupied time interval of a grid cell is determined by the union of these time intervals.

The main advantage of this method is the conservation of computing resources. As implied by Lines 6-8, if all the other aircraft paths are mapped and stored in the grid, only the path of the observed aircraft needs to be computed at each step. This method is well-suited for scenarios involving a large number of aircraft. In practice, all dynamic obstacles can be mapped in advance before conducting a search. However, similar to other grid-based algorithms, the precision and performance of this method are significantly influenced by the chosen grid size. If the grid size is excessively large, false alarms may occur frequently. A flexible grid size may be helpful in practice.

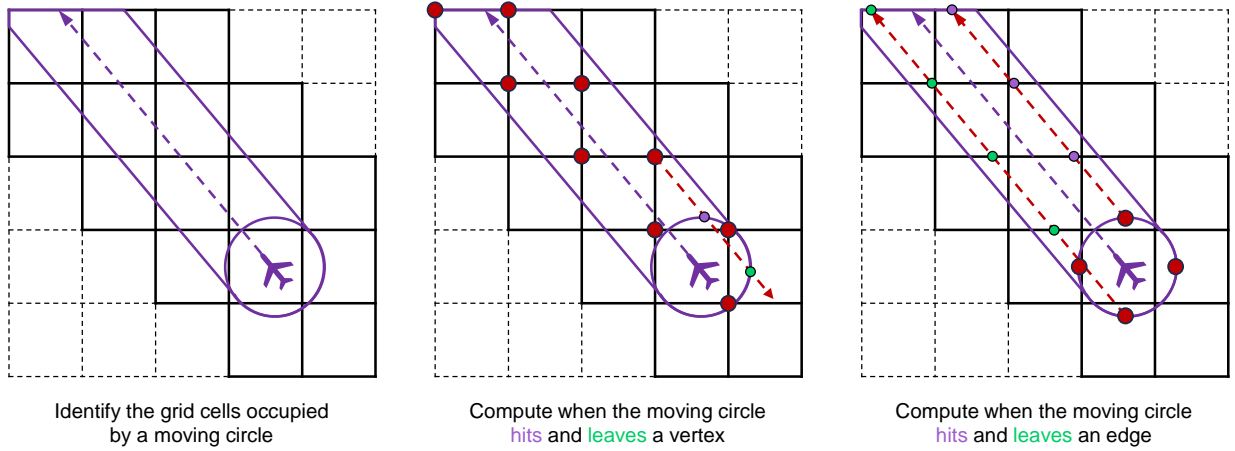


Figure 5: Computation of occupied time intervals (mapToGrid).

4.2.3. Conflict detection based on conflict zones

The first two conflict detection methods mentioned above resemble the line of sight, but for dynamic obstacles. To generate a solution space, each grid cell has to be inspected through conflict detection to determine whether the path between it and the current node is obstructed by dynamic obstacles. However, similar to the line of sight, the nodes around the current node may undergo repeated examination, indicating that it would be beneficial to achieve the field of view for dynamic obstacles as well.

Inspired by HIPS [37], conflict zones can be constructed to indicate where conflicts may arise if the aircraft only changes its heading, as shown in Figure 6. The path is like a ray casting from the current location and the conflict zone can be regarded as a static obstacle. Different from the original HIPS, we incorporate the turning angle constraint (AOV) and the flight duration into the conflict zone computation. Considering that the crossing aircraft may have multiple path segments, the flight duration is the duration for which the crossing aircraft will continue flying in its current heading. The front curve of the limited conflict zone (red region) can be mapped to create obstacle grid cells, and then shadowcasting can be applied to create the field of view for dynamic obstacles as well.

In summary, the zone-based conflict detection method contains two main steps. First, for the current node, dynamic obstacles are transformed into static obstacles using the conflict zones. Second, the shadowcasting is executed to find all conflict-free nodes to generate a solution space. This method can be combined with visibility checks in Section 4.1 and the shadowcasting only needs to be performed once for each current node. Therefore, the procedure in Algorithm 1 requires slight revision since the *for* loop for conflict detection is unnecessary.

Algorithm 4 describes the procedure of conflict zone computation. The flight duration $T_{l,m} = \emptyset$ in Line 6 means that the path segment l_m has already been traversed by the crossing aircraft by the time the observed aircraft reaches the node n . The conflict heading range represents the extent of the conflict zone. Instead of considering the entire AOV, we focus solely on the headings that could potentially lead to a conflict.

The conflict heading range can be computed based on the velocity obstacles in the Solution Space Diagram (SSD)

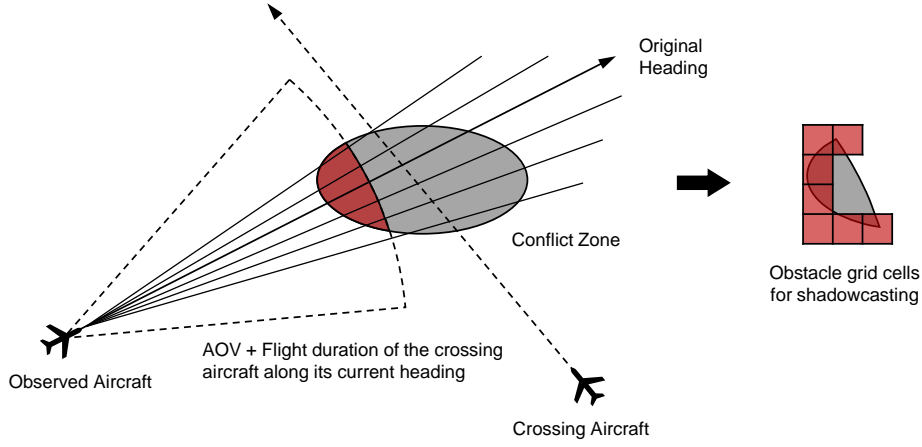


Figure 6: Construction of a conflict zone, combined with AOV and flight duration.

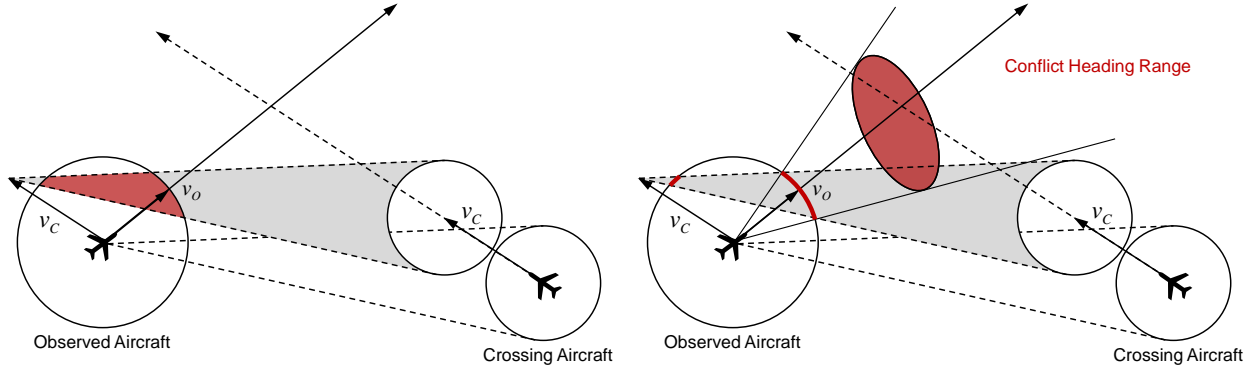


Figure 7: Computation of conflict heading ranges based on the triangular velocity obstacle in SSD.

[41, 73], as shown in Figure 7. The circle surrounding the crossing aircraft denotes the safe separation, while the circle around the observed aircraft has a radius of v_o . v_o and v_c are the velocities of the observed and crossing aircraft, respectively. The headings outside the velocity obstacle do not need to be considered for computing the conflict zones. Please note that a velocity obstacle may produce two different conflict heading ranges due to the four intersections between the obstacle triangle and the velocity circle. For each heading θ_i within the heading ranges, the time duration and position of the conflict can be computed.

As depicted in Figure 8, if the start time t_0 of the crossing aircraft's path segment exceeds the start time $g(n)$ of the observed aircraft, the initial position of the crossing aircraft should be back-propagated to synchronize their start times. This alignment helps the computation of the conflict duration T_i . If $T_i \cap T_{l,m} \neq \emptyset$, the corresponding conflict position will be appended to the front curve list $P_{l,m}$. A line drawing algorithm can then be used to map the curve onto the grid. Ultimately, the shadowcasting is leveraged to simultaneously scan both visible and conflict-free nodes, as depicted in Line 21.

This conflict-zone-based approach offers the advantage of eliminating the need to conduct conflict detection for

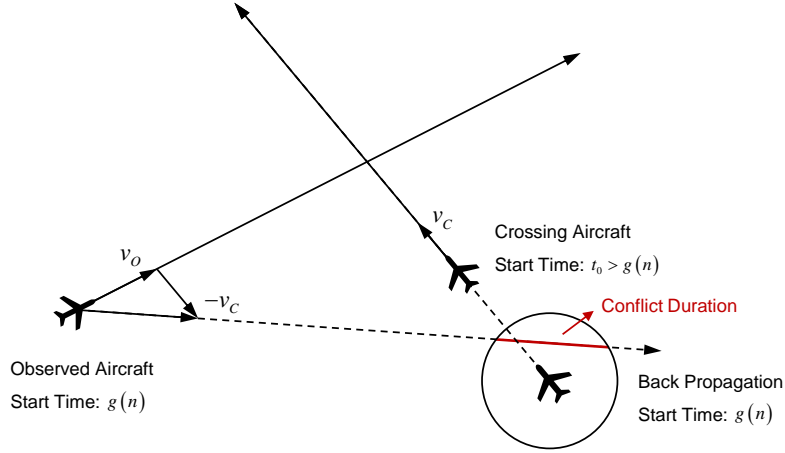


Figure 8: Computation of conflict duration.

Algorithm 4 Conflict detection based on conflict zones

Require: current node n , current heading θ , maximum turning angle θ_0

```

1: function zoneConflictDetection( $n, \theta$ )
2:   for each other aircraft  $m$  do
3:     for each path segment  $l_m$  do
4:       front curve  $P_{l,m} \leftarrow \emptyset$ 
5:        $T_{l,m} \leftarrow \text{computeFlightDuration}(l_m) \cap [g(n), \infty)$ 
6:       if  $T_{l,m} = \emptyset$  then
7:         continue
8:       end if
9:        $AOV(n) \leftarrow [\theta - \theta_0, \theta + \theta_0]$ 
10:       $[\theta_{n,1}, \theta_{n,2}] \leftarrow \text{computeConflictHeadingRange}(n, l_m)$ 
11:      for  $\theta_i \in AOV(n) \cap [\theta_{n,1}, \theta_{n,2}]$  do
12:         $T_i \leftarrow \text{computeConflictDuration}(n, \theta_i, l_m)$ 
13:        if  $T_i \cap T_{l,m} \neq \emptyset$  then
14:           $p_i \leftarrow \text{computeConflictPosition}(n, \theta_i, T_i \cap T_{l,m})$ 
15:           $P_{l,m} \leftarrow P_{l,m} \cup \{p_i\}$ 
16:        end if
17:      end for
18:       $Grid \leftarrow \text{mapCurveToGrid}(P_{l,m}, Grid)$ 
19:    end for
20:  end for
21:   $N_{reachable} \leftarrow \text{shadowcasting}(n, AOV(n))$ 
22:  return  $N_{reachable}$ 
23: end function

```

each grid cell while also exhibiting good compatibility with visibility check methods (e.g., shadowcasting). However, the discretization of headings in Algorithm 4 may introduce some degree of precision loss, especially when the conflict zone is distant from the current node.

5. Solution space path planning

In Section 4, we introduced the details of solution space generation at each search step, and, in this section, we will illustrate the main procedures and algorithms for Solution Space Path Planning (SSPP). Two versions of SSPP are proposed: *SSPPV* and *SSPPE*. They differ in how search nodes are defined: *SSPPV* treats each vertex/point (i.e., a grid cell) as a node, whereas *SSPPE* treats each pair of vertices/points (i.e., an edge) as a node. In this section, we also explore a potential extension to SSPP that accounts for robustness by jointly optimizing delay and separation.

5.1. *SSPPV: Vertex-based SSPP*

A simple implementation of *SSPPV* is to replace the eight adjacent neighbors in traditional A* with a solution space for node expansion, as shown in Algorithm 5. $S(n)$ can be regarded as extended neighbors and represents all reachable nodes from the current node n . This approach enables any-angle path planning [24], which allows any-angle turns at graph vertices to generate straighter paths without post-hoc smoothing. This property is particularly suitable for aircraft that cannot make sharp turns. Certainly, the turning angle constraint should be satisfied and $S(n)$ inherently incorporates this requirement (AOV). We also introduce $depth(n)$ to indicate the depth of a node n , allowing ATCos to restrict the depth of the search tree based on the maximum number of rerouting points k ($k \geq 0$). Since the nodes in $S(n)$ are reachable from the current node n , it is possible for n to be the true or best parent of a node n' in $S(n)$. From Line 13 to Line 24, a comparison is conducted between the current node n and the current best parent of n' to determine which node is a better parent for n' . This operation is intended to expand and rewire the search tree to achieve a growing and straight tree structure. The closed nodes are excluded in $S(n)$ because, once a node is closed, the best path from the start node to that node is considered to have been found (A* property). Thus, it is meaningless to still consider the closed nodes as potential children of the current node.

The solution space generated at each step appears to suggest that all possibilities contributing to the discovery of optimal paths will be explored during the search. However, this is not the case, as the generated solution space is also influenced by the “incoming” heading θ . Due to the AOV, different incoming headings will cover different following headings. It means that a node n' may be unreachable from a closed node n and its best parent $parent(n)$, but it may be reachable from n and a different parent $parent(n)'$. Unlike traditional A*, the node expansion in SSPP is not only associated with the node position but also with its parent. The closed nodes with their parents in *SSPPV* form a fixed search tree, and then the `generateSolutionSpace(n, θ)` further explores the possibilities expanding from the fixed tree. Therefore, *SSPPV* can only find optimal paths within its exploration range and may sometimes fail to find a path even when one exists.

5.2. *SSPPE: Edge-based SSPP*

To address this issue in *SSPPV*, we develop *SSPPE*, as shown in Algorithm 6. As the node expansion in *SSPPV* involves both nodes and their parents, we treat a pair of points as a search node $l = [n_1, n_2]$ in *SSPPE*. Each node corresponds to a specific incoming heading. The real cost of a node in *SSPPE* is $g(l) = g(parent(l)) + g(n_1, n_2)$ and the

Algorithm 5 Vertex-based Solution Space Path Planning (SSPPV)

Require: start node n_s , target node n_t

- 1: $depth(n_s) \leftarrow 0$, $open \leftarrow \{n_s\}$, $closed \leftarrow \emptyset$
- 2: **while** $open \neq \emptyset$ **do**
- 3: $n \leftarrow \arg \min_{n \in open} f(n)$
- 4: $open \leftarrow open \setminus \{n\}$, $closed \leftarrow closed \cup \{n\}$
- 5: **if** $n = n_t$ **then**
- 6: **return** $pathTo(n)$
- 7: **end if**
- 8: **if** $depth(n) > k$ **then**
- 9: **continue**
- 10: **end if**
- 11: $\theta \leftarrow computeHeading(parent(n), n)$
- 12: $S(n) \leftarrow generateSolutionSpace(n, \theta)$
- 13: **for each** node $n' \in S(n)$ **do**
- 14: **if** $n' \in closed$ **then**
- 15: **continue**
- 16: **end if**
- 17: $g_{new} \leftarrow g(n) + g(n, n')$
- 18: **if** $parent(n') = null$ or $g(n') > g_{new}$ **then**
- 19: $parent(n') \leftarrow n$, $g(n') \leftarrow g_{new}$
- 20: $f(n') \leftarrow g_{new} + h(n')$
- 21: $depth(n') \leftarrow depth(n) + 1$
- 22: insert or update n' in $open$
- 23: **end if**
- 24: **end for**
- 25: **end while**
- 26: **return** $null$

total cost is $f(l) = g(l) + h(n_2)$. Once a node is closed, the best path from the start point to n_2 via n_1 is considered to have been found. If l is the first closed node containing n_2 , the best path to n_2 is also determined. This demonstrates that if l is closed, the remaining time T in Algorithm 1 is maximized, resulting in the largest search region from l . However, this approach transforms a 2D search space \mathbb{R}^2 into a 4D search space $\mathbb{R}^2 \times \mathbb{R}^2$, as each node comprises a pair of points. The speed of SSPPE may be significantly slower than that of SSPPV.

However, SSPPE is still not truly optimal. When a node is closed, its earliest arrival time (i.e., the lowest g-value) is fixed. Although this typically provides the largest feasible solution space for the next waypoint, arriving at a node as early as possible does not guarantee that conflicts with dynamic obstacles along subsequent paths can be resolved. For example, as shown in Figure 9, consider a case where point C is unreachable from node AB (a pair of points) when the arrival time at B is 13:00, but becomes reachable if the arrival time is delayed to 13:10. In such situations, the earliest arrival time does not produce a *complete* solution space that represents all possibilities from AB , indicating that SSPPE is not optimal. Interestingly, compared to TO-AA-SIPP, optimal any-angle path planning becomes more challenging when waiting actions are not permitted.

Essentially, both SSPPV and SSPPE are based on A* search. The complexity of A* can be described as $O(b^d)$

Algorithm 6 Edge-based Solution Space Path Planning (SSPPE)

Require: start node n_s , target node n_t , heading θ_s

```
1: initialization( $n_s, \theta_s$ )
2: while  $open \neq \emptyset$  do
3:    $l = [n_1, n_2] \leftarrow \arg \min_{l \in open} f(l)$ 
4:    $open \leftarrow open \setminus \{l\}, closed \leftarrow closed \cup \{l\}$ 
5:   if  $n_2 = n_t$  then
6:     return pathTo( $l$ )
7:   end if
8:   if  $depth(l) > k$  then
9:     continue
10:  end if
11:   $\theta \leftarrow \text{computeHeading}(n_1, n_2)$ 
12:   $S(l) \leftarrow \text{generateSolutionSpace}(n_2, \theta)$ 
13:  for each  $l' = [n_2, n'] \in S(l)$  do
14:    if  $l' \in closed$  then
15:      continue
16:    end if
17:     $g_{new} \leftarrow g(l) + g(n_2, n')$ 
18:    if  $parent(l') = \text{null}$  or  $g(l') > g_{new}$  then
19:       $parent(l') \leftarrow l, g(l') \leftarrow g_{new}$ 
20:       $f(l') \leftarrow g_{new} + h(n')$ 
21:       $depth(l') \leftarrow depth(l) + 1$ 
22:      insert or update  $l'$  in  $open$ 
23:    end if
24:  end for
25: end while
26: return null
```

Algorithm 7 SSPPE Initialization

```
1: function initialization( $n_s, \theta_s$ )
2:    $open \leftarrow \emptyset, closed \leftarrow \emptyset$ 
3:    $l_s \leftarrow [n_s, n_s], depth(l_s) \leftarrow 0$ 
4:    $S(l_s) \leftarrow \text{generateSolutionSpace}(n_s, \theta_s)$ 
5:   for each  $l' = [n_s, n'] \in S(l_s)$  do
6:      $parent(l') \leftarrow l_s, g(l') \leftarrow g(n_s, n')$ 
7:      $f(l') \leftarrow g(l') + h(n')$ 
8:      $depth(l') \leftarrow depth(l_s) + 1$ 
9:     insert  $l'$  in  $open$ 
10:  end for
11: end function
```

where b is the branching factor and d is the depth of the shallowest solution. In similar scenarios, SSPPV and SSPPE produce solutions with comparable depths, and the key difference between them lies in their branching factors. Let n denote the number of cells within the solution space. Then, the branching factor for SSPPV is n , while for SSPPE it is n^2 (ignoring constraints such as turning angle limitations). Therefore, their complexities can roughly be expressed as $O(n^d)$ and $O(n^{2d})$, respectively.

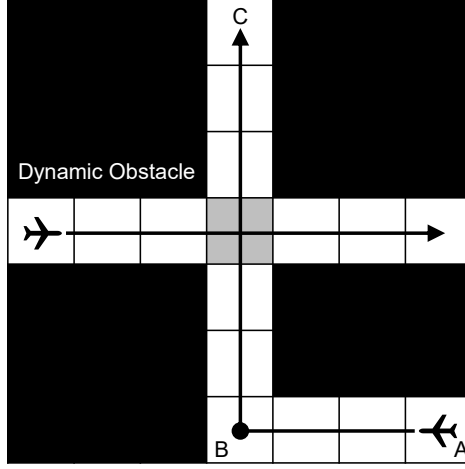


Figure 9: Example illustrating why SSPPE is not optimal.

5.3. Trade-off between delay and separation

The original objective of SSPP, including both SSPPV and SSPPE, is to find time-optimal conflict-free paths. This means that only the node with the lowest time delay is selected from *open* and moved to *closed* at each step. However, in practice, ATCos may favor more robust solutions [40]. In this section, we explore potential extensions to SSPP by taking robustness into account.

Idris et al. [74, 75] introduced the concept of trajectory flexibility and proposed two metrics for it: robustness and adaptability. Klomp et al. [40] further developed metrics for point-based, trajectory-based, sector-based and control-based robustness. However, calculating these metrics often requires generating a complete “trajectory” solution space, which typically demands significant computing resources and time. While SSPP computes the “next-point” solution space for each closed node, the “trajectory” solution space it explores remains limited due to A* search.

Since disturbances may arise from the maneuvering behavior or uncertainties of aircraft, robustness can be measured by the separation distance between them. A larger separation indicates a greater ability to tolerate such disturbances. Similarly, adaptability can be assessed by the remaining allowable time delay. The time-optimal trajectory suggests that the aircraft has the maximum available maneuvering space to adjust its current flight plan. Therefore, we can redesign the cost function of SSPP to minimize the time delay and maximize the separation distance:

$$f_{total}(n) = g_{total}(n) = w_1 \cdot g_{delay}(n) + w_2 \cdot g_{sep}(n) = w_1 \cdot \frac{t_{delay}(n)}{t_{max_delay}} + (1 - w_1) \cdot \frac{d_{min_sep}}{d_{sep}(n)} \quad (5)$$

where w_1 and w_2 are the objective weights within $[0, 1]$, $t_{delay}(n)$ is the delay experienced upon arrival at the node n and t_{max_delay} is the maximum allowable time delay. $t_{delay}(n)$ can be calculated by

$$t_{delay}(n) = g(n) + h(n) - h(n_s) = f(n) - h(n_s) \quad (6)$$

where, as defined in previous sections, n_s is the start node, $g(n)$ is the real flight time from the start node to the node n and $h(n)$ is the estimated flight time from the node n to the target node. $d_{sep}(n)$ is the separation distance between $pathTo(n)$ and other crossing aircraft and d_{min_sep} is the minimum separation. $d_{sep}(n)$ can be calculated by

$$d_{sep}(n) = \min\{d_{sep}(parent(n)), d_{sep}(parent(n), n)\} \quad (7)$$

where $d_{sep}(parent(n), n)$ is the separation between the path segment $[parent(n), n]$ and other aircraft. The advantage of this design is that the ranges of $g_{delay}(n)$ and $g_{sep}(n)$ are both scaled to $[0, 1]$, eliminating the need to account for differences in units. Moreover, both $g_{delay}(n)$ and $g_{sep}(n)$ are *monotonic* functions for a trajectory; they never decrease as the depth of the waypoints increases.

For robust SSPPV, two functions related to cost computation in Algorithm 5 require modifications:

$$g_{new} \leftarrow w_1 \cdot \frac{g(n) + g(n, n') + h(n') - h(n_s)}{t_{max_delay}} + (1 - w_1) \cdot \frac{d_{min_sep}}{\min\{d_{sep}(n), d_{sep}(n, n')\}} \quad (8)$$

and $f(n') \leftarrow g_{new}$. The rest of the procedure and code remain the same. Similarly, in robust SSPPE,

$$g_{new} \leftarrow w_1 \cdot \frac{g(l) + g(n_2, n') + h(n') - h(n_s)}{t_{max_delay}} + (1 - w_1) \cdot \frac{d_{min_sep}}{\min\{d_{sep}(l), d_{sep}(n_2, n')\}} \quad (9)$$

where $l = [n_1, n_2]$ and $f(l') \leftarrow g_{new}$. According to Equation 7,

$$d_{sep}(l) = \min\{d_{sep}(parent(l)), d_{sep}(n_1, n_2)\} \quad (10)$$

If $w_1 = 1$, the robust SSPP will revert to its basic version, focusing only on finding time-optimal conflict-free paths. This is because t_{max_delay} is a positive constant and $f_{total}(n) = g_{delay}(n)$ increases monotonically with $f(n)$. In this case, the trajectory separation may approach the minimum separation since the algorithm strives to find trajectories with minimal deviation. If $w_1 = 0$, the robust SSPP will find paths with the largest possible separation, but the solutions may approach the maximum allowable time delay. ATCos should be allowed to adjust the weights to balance these two objectives based on their operational needs.

Since $d_{sep}(n)$ involves computing the separation distance, it is ideally suited for the distance-based conflict detection. For the other two methods, perhaps a different cost function design is needed. In this article, we only explore one of the possibilities for extensions to SSPP. Essentially, the cost function affects which node is selected from the solution space $S(n)$. A more complex function incorporating additional factors can also be developed.

6. Case study

6.1. Experiment setup

To analyze the performance of the proposed algorithms, we selected the Delta sector in the Maastricht Upper Area Control Centre (MUAC) airspace above the Netherlands as a case study. A single sector, rather than a multi-sector coordination environment, was chosen because our focus is on tactical ATC rather than air traffic flow management. The algorithms were implemented in a web-based ATC simulator¹ that we developed using JavaScript and the experiments were performed on Node.js v22.19.0 on a laptop with 2.30GHz Intel Core i7-11800H and 16 GB RAM.

In this study, we do not directly compare SSPP with existing algorithms because they are not fully applicable to the specific problem we address. For example, A* and Theta* cannot handle dynamic obstacles, SIPP often produces zigzag paths unsuitable for aircraft motion, and AA-SIPP, TO-AA-SIPP and Zeta*-SIPP do not consider constraints such as turning angle limitations and maximum allowable time delay. Therefore, rather than conducting a direct comparison, we extract and integrate the key distinguishing elements of these algorithms for analysis: distance-based and time-interval-based conflict detection. The former is widely adopted in the ATC domain [20], whereas the latter is commonly applied in the path-planning field (i.e., SIPP-based planners). Additionally, the overall goal of this study is not to develop the fastest algorithm; rather, it aims to propose a new perspective on algorithm design to support ATCo decision-making (e.g., interpretable, reliable, near-optimal, and sufficiently fast). Therefore, all comparisons are conducted within the solution space path planning framework. To enable real-time and seamless human-machine interaction, the computational latency of the proposed algorithms should ideally be bounded by human response time, which is generally considered to lie between 100 and 200 ms [76].

Drawing on our experience in ATC, we chose to set the algorithm parameters like Table 1. The minimum horizontal separation 5 nmi is determined by the minimum separation standard. The maximum allowable time delay is set to 300 seconds because the resulting initial solution space nearly covers the entire sector. The turning angle limitation is set to 60° to reflect typical aircraft maneuverability. The minimum distance between waypoints is set to 10 nmi (twice the minimum separation standard) based on discussions with ATCos. The maximum number of rerouting waypoints is set to either 1 or 5 to evaluate the extent of improvement achievable by allowing additional rerouting points in path planning. The grid size is set to 5 or 2.5 nmi, allowing ATCos to more easily observe whether two aircraft are safely separated on grids. Finally, the heading discretization is set to 0.5° for zone-based conflict detection, as this resolution supports the accurate calculation of conflict zones.

There were about 38 entry and exit points for the Delta sector. We randomly generated pairs of these points to be start and target points for aircraft. By default, the aircraft flew directly to their designated target points. The flight level was set to FL350, with a random speed from Mach 0.71 to Mach 0.83. All aircraft entered the sector simultaneously and executed the proposed path-planning algorithm sequentially. The aircraft that performed the algorithm first were

¹Demo: <http://dronectr.tudelft.nl/> (ID: SSPP).
Code: <https://github.com/yiyuanzou/sspp>.

Table 1: Algorithm parameters.

Parameter	Value
Minimum horizontal separation	5 nmi
Maximum allowable time delay	300 s
Turning angle limitation	60°
Minimum distance between waypoints	10 nmi
Maximum number of rerouting waypoints	1 or 5
Grid size	5 or 2.5 nmi
Heading discretization	0.5°

treated as dynamic obstacles for the subsequent aircraft. In practice, we can adapt a first-come-first-served principle. If an aircraft could not identify a conflict-free path, it would proceed along its original direct route and be marked as failed. Here, the “conflict-free” means that the minimum separation standard is not violated. To avoid generating unrealistic flights, the following rules were applied:

- 1) The start points of aircraft should be at least 7.5 nmi apart to ensure that no loss of separation occurs at the beginning. This value was determined based on the minimum separation standard with a 50% buffer.
- 2) There should be no conflict within 2 minutes when aircraft follow direct routes to their target points. This value was chosen because the short-term conflict alert in ATC is typically 2 minutes in advance.
- 3) The start and target points of aircraft should not be located on the same edge of the sector.
- 4) To ensure a flight impacts the sector, the length of its direct route was set to exceed 30 nmi.
- 5) The direct route should be within the sector without intersecting its boundary.

The algorithms were assessed with aircraft numbers ranging from 2 to 20. For each aircraft number, 100 random scenarios were generated. The maximum number was set to 20 because, after applying the first filtering rule for entry and exit points, only 27 usable points remained for scenario generation. Moreover, since all aircraft operated at the same flight level (FL350) and their start-target pairs were randomly assigned, the resulting flight trajectories could be highly complex with many intersections, representing extreme and challenging traffic conditions for human ATCos. As shown in Figure 10, before rerouting, when the number of aircraft reaches 20, the number of intersections can increase to around 100. Additionally, in real-world operations, traffic density in the MUAC Delta sector rarely exceeds 20 aircraft at the same flight level at any given time. Note that scenarios with larger numbers of aircraft were not constructed by extending smaller ones; instead, each was created independently from scratch. The success rate of SSPP for each scenario was computed as the number of aircraft that successfully find a conflict-free path divided by the total number of aircraft. This metric was adopted because the path-planning algorithm was applied sequentially to each individual aircraft, rather than simultaneously to multiple aircraft.

In normal scenarios, there is no static obstacle in the sector. However, if hazardous weather appears, a no-fly zone may need to be established. Therefore, we defined two different airspace conditions: one with no static obstacle and another with a single obstacle located in the sector center. Figure 11 presents the screenshots of a random scenario featuring 12 aircraft. The radar labels are blue, indicating that these aircraft are under automation control. The blue

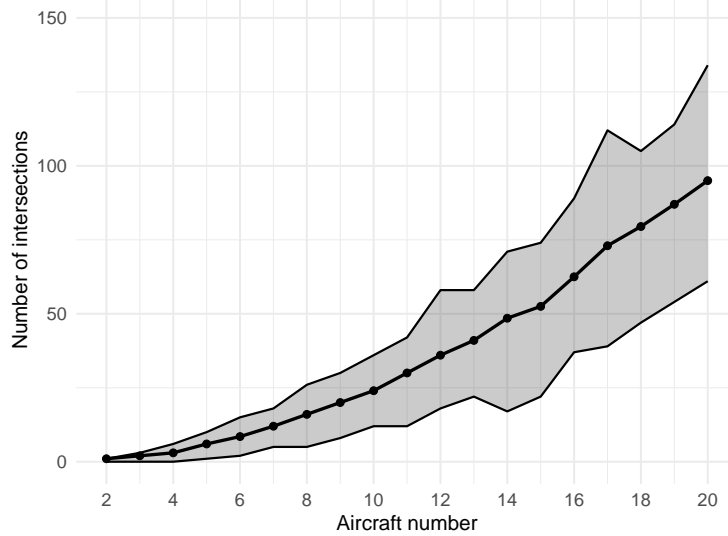


Figure 10: Minimum, median, and maximum number of intersections prior to rerouting. The shaded region indicates the range between minimum and maximum values.

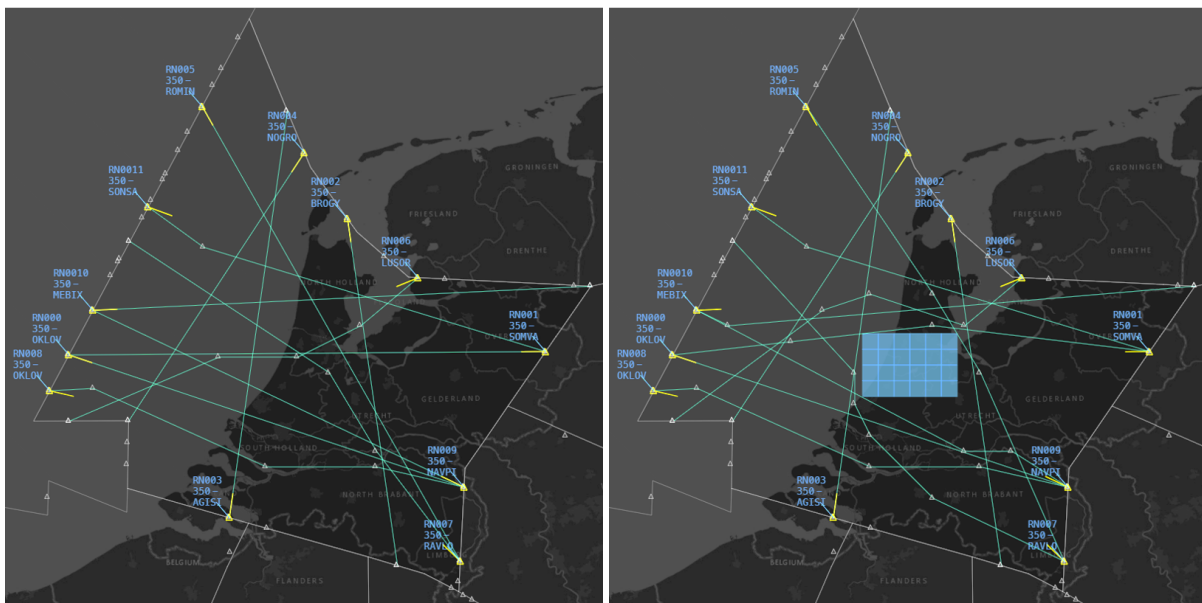


Figure 11: Screenshots of a random scenario featuring 12 aircraft.

rectangular region is a no-fly zone (static obstacle) that all aircraft need to avoid entering. The paths were generated by SSPP based on conflict zones, serving as an example. Figure 12 visualizes the internal process of this algorithm. The green ellipse represents the maximum allowable delay constraint, integrating the AOV and minimum waypoint distance constraints. The green grid cells represent search nodes explored by the algorithm, with light yellow lines representing the branches connecting these nodes. The red regions are conflict zones and the one under the mouse cursor is caused by the aircraft “RN003”. All areas within the green ellipse, except for the green cells, are considered

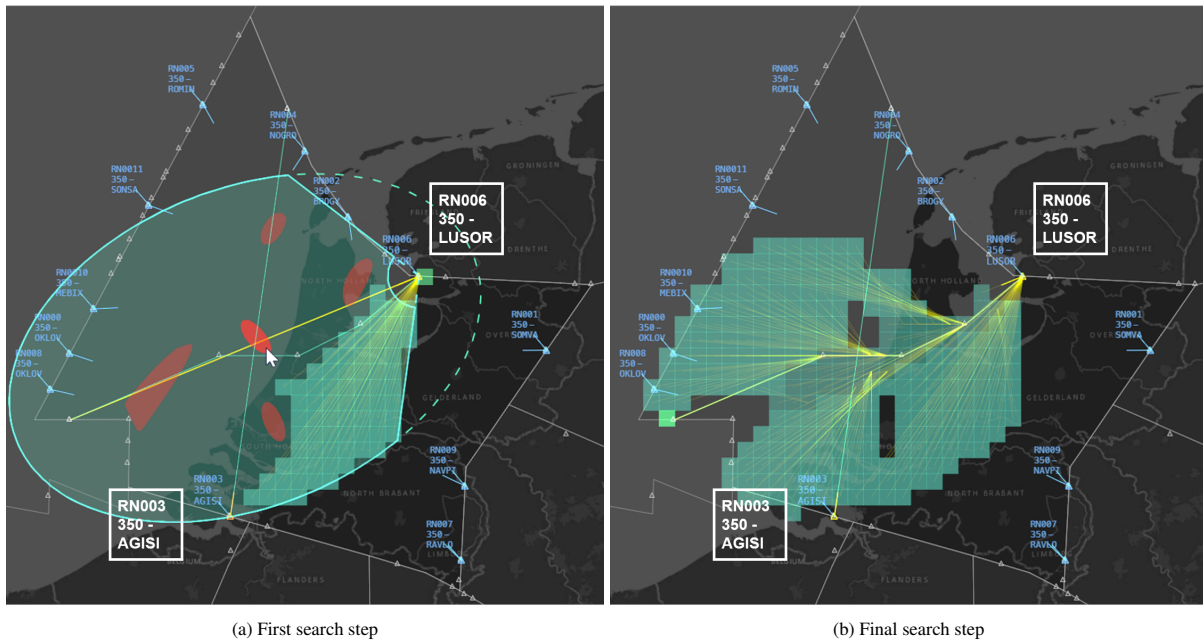


Figure 12: Screenshots of the internal process of SSPP using conflict zones.

unreachable due to conflicts. To reduce visual clutter, the red grid cells indicating unreachable areas are hidden. Note that the conflict zones are generated exclusively for the zone-based conflict detection method. The distance-based and time-interval-based conflict detection methods only specify whether nodes are reachable or not.

6.2. Performance analysis

6.2.1. SSPPV and SSPPE for minimizing delay

Figure 13 presents the results of SSPPV and SSPPE in minimizing delay (weight = 0) under the three conflict detection methods: Distance-based (D), Time-interval-based (T), and Zone-based (Z). From Figure 13a, as the number of aircraft increases, the potential for conflicts rises, causing more aircraft to reroute and resulting in increased delay. Since the algorithms aim to minimize delay, the maximum turning angle tends to be smaller when fewer aircraft are present, as shown in Figure 13b. Generally, the average delay generated by the algorithms are less than 45 seconds. Among the conflict detection methods, the time-interval-based method (T) is the most conservative, consistently producing higher delay and lower success rates than the others. In contrast, the distance-based method (D) is the most accurate, achieving the lowest delay and highest success rates. When the grid size is 5 nmi, the time-interval-based method overall adds a 1.95% buffer to the average separation compared to the distance-based method.

In most cases, SSPPV and SSPPE yield comparable optimization results; however, surprisingly, SSPPE-T generates higher delay than SSPPV-T although SSPPE explores more possible states. This is because SSPPE generally has a higher success rate than SSPPV (see Figure 13c), and successful rerouting can result in greater delay compared to direct paths (recall that when rerouting fails, it defaults to the direct path). The time-interval-based (T) method further

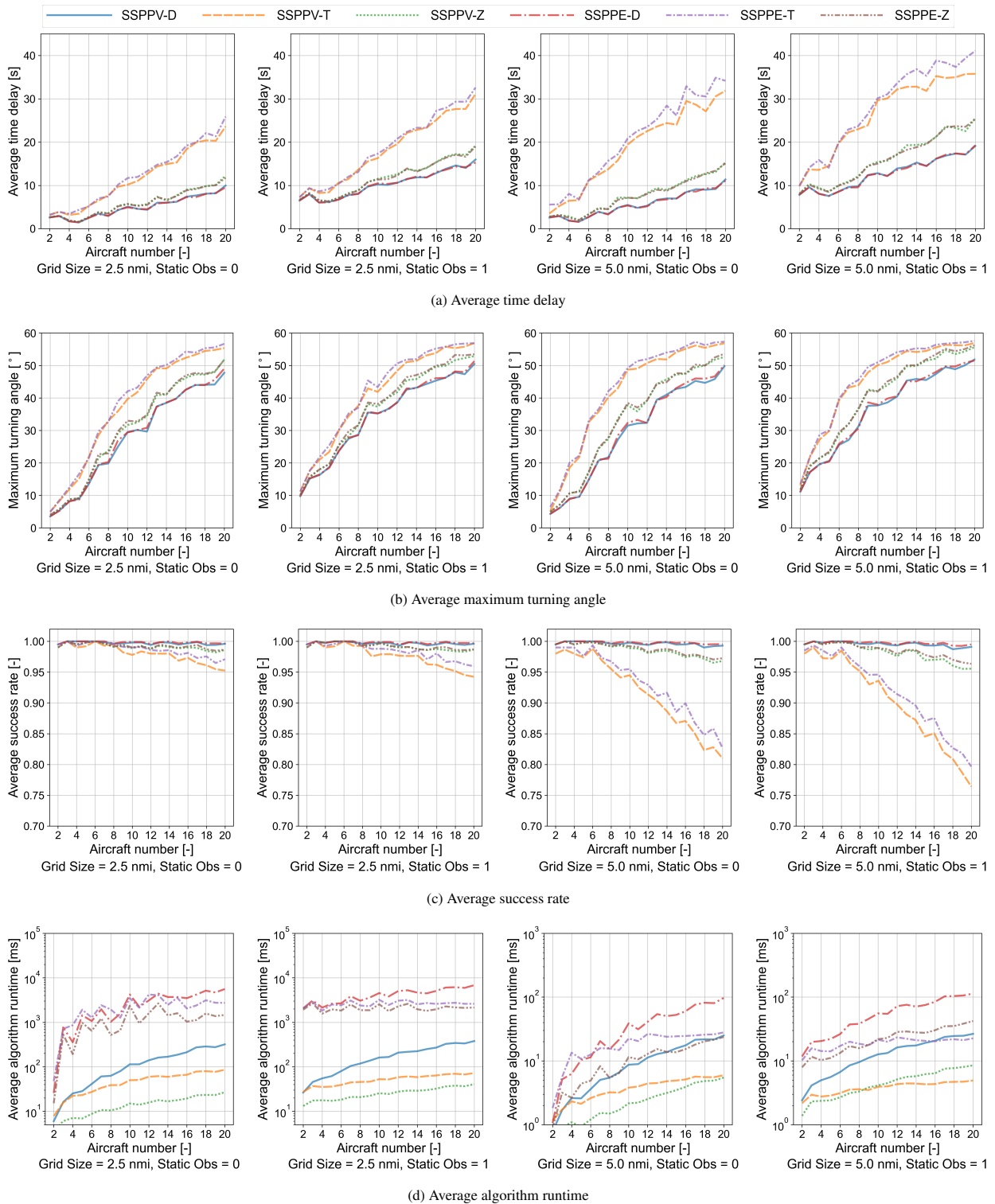


Figure 13: Algorithm results with fixed rerouting waypoints at 5 and weight at 0. “Static Obs = 1” denotes the presence of a static obstacle at the sector center, as shown in the right plot of Figure 11.

Table 2: Average runtime of solution space generation [ms].

Condition	Distance-based	Time-interval-based	Zone-based
Grid Size = 2.5 nmi, Static Obs = 0	3.2525	1.1234	0.3629
Grid Size = 2.5 nmi, Static Obs = 1	2.2700	0.6264	0.3035
Grid Size = 5.0 nmi, Static Obs = 0	0.8129	0.1750	0.1583
Grid Size = 5.0 nmi, Static Obs = 1	0.5844	0.1116	0.1716

amplifies this effect. However, SSPPE-Z occasionally has a lower success rate than SSPPV-Z. This is possibly due to the domino effect caused by the first-come-first-served strategy, where an aircraft that fails to reroute may make it easier for subsequent aircraft to find conflict-free paths.

The results also indicate that a smaller grid size can significantly improve the success rate but comes at the cost of a much higher algorithm runtime, as shown in Figure 13d. When the grid size is 2.5 nmi, the average runtime of SSPPE is generally more than 1,000 ms, while at a grid size of 5 nmi, the runtime drops to less than 100 ms. SSPPV is considerably faster than SSPPE, with a runtime of only about 5-10 ms when the grid size is 5 nmi. The zone-based method (Z) leads to the lowest runtime in most scenarios, with SSPPV-Z remaining below 100 ms (the typical lower bound of human response time) across all experiments, showcasing its potential for conflict-free path planning and real-time “what-if” probing.

For further comparison, Table 2 presents the average runtime of solution space generation using different conflict detection methods. The computation of the solution space is generally fast. These results can also serve as a reference for those who wish to only implement the solution space to support human control. When the grid size is smaller, the advantage of the zone-based conflict detection method becomes more pronounced. This is because the conflict zones can facilitate the implementation of the shadowcasting for dynamic obstacles, helping to avoid repeated examinations of nodes surrounding the current node. However, due to the additional calculation of the conflict zones, the zone-based method becomes slower than the time-interval-based method when the grid size is larger.

Figure 14 illustrates the results when the maximum number of rerouting waypoints is set to 1. In this case, SSPP simplifies to TSR-based path planning, allowing only one intermediate rerouting point. It is evident that the success rate drops significantly compared to when the rerouting waypoints are set to 5 (see Figure 13 (c)). This indicates that as the number of aircraft increases, rerouting them with multiple waypoints becomes increasingly necessary, and TSR with only one rerouting point may be insufficient to support ATCos effectively. When the rerouting point is 1, SSPPV and SSPPE generate identical paths because each node has only one incoming heading from the start point. However, SSPPE is generally slower than SSPPV due to differences in their initialization processes and data structure. SSPPE needs to create a 4D array to store its search nodes.

Figure 15 presents the results across different grid size settings. The impact of grid size on success rate depends on scenario complexity. When only two aircraft are involved, all methods maintain near-perfect success rates regardless of grid size. As traffic density increases (i.e., more dynamic obstacles) or static obstacles are added, the success rates of all methods decline with increasing grid size. The magnitude of this decline differs across method categories: the time-

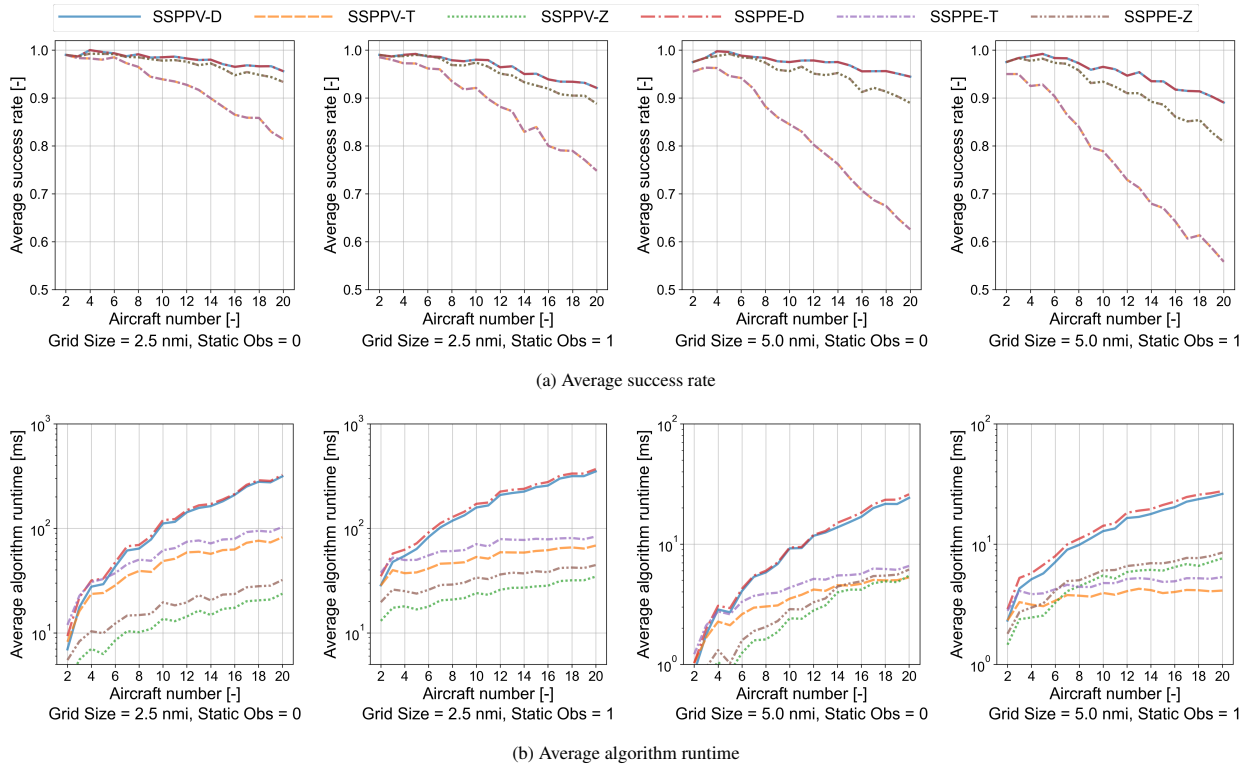


Figure 14: Algorithm results with fixed rerouting waypoints at 1 and weight at 0.

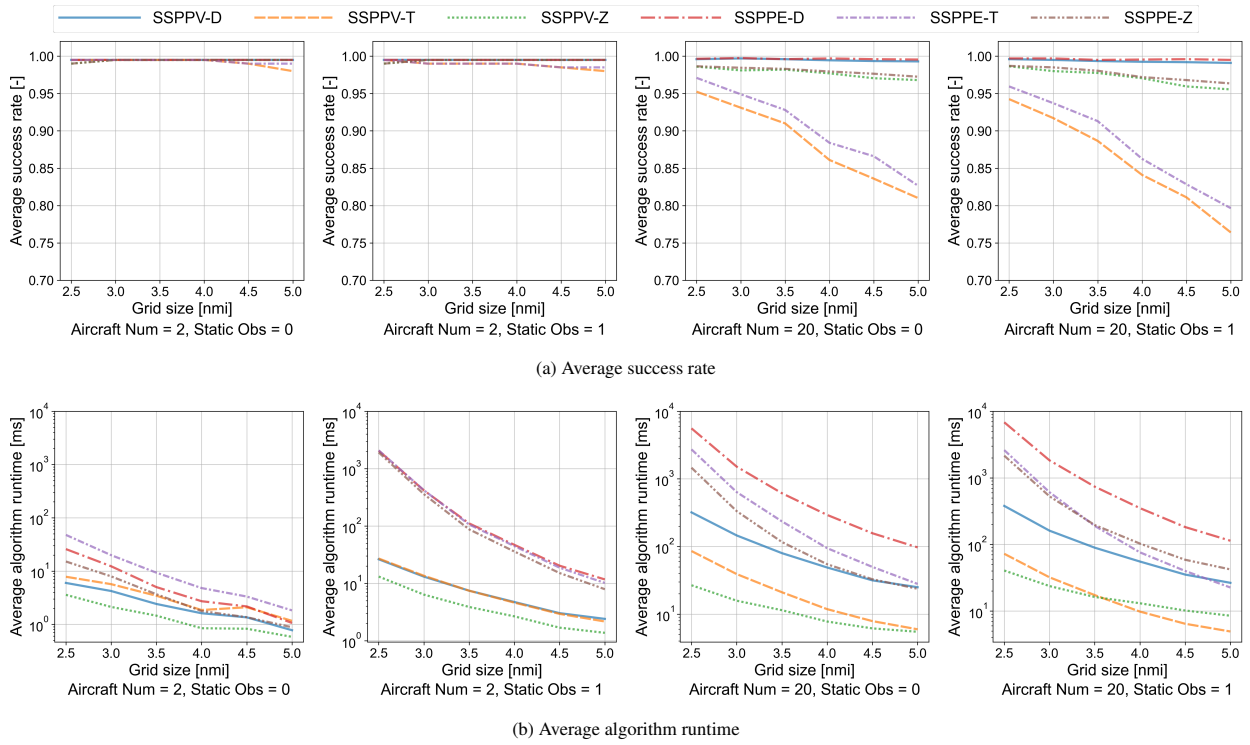


Figure 15: Algorithm results with fixed rerouting waypoints at 5 and weight at 0, and varying grid sizes.

interval-based method is the most sensitive to grid size changes, the zone-based method exhibits moderate sensitivity, and the distance-based method remains comparatively robust. The algorithm runtime consistently decreases as grid size increases, since larger grids lead to smaller search space and reduce the overall search effort. Within this general trend, the zone-based method achieves the lowest runtime in most scenarios. When the grid size exceeds 3.5 nmi, the time-interval-based method may become slightly faster than the zone-based method in high-traffic conditions.

6.2.2. SSPPV and SSPPE for delay and separation trade-offs

Figure 16 presents the results of SSPPV and SSPPE for delay and separation trade-offs. Note that in this research, we only propose an extension to SSPP using distance-based conflict detection (SSPPV-D and SSPPE-D). We chose 2 and 20 aircraft, along with a grid size of 5 nmi, as examples. The weight here refers to the weight of separation in the objective function. From Figures 16a and 16b, as the weight increases, both the average separation and delay increase. This change becomes more apparent when the weight is 1, where the algorithms only aim to maximize separation rather than minimize delay. When the number of aircraft is 2, the trade-off between separation and delay is clearly observed, demonstrating the effectiveness of the robust SSPP. However, when the number of aircraft increases to 20, the loss of separation caused by pathfinding failures greatly reduces the benefits gained from optimizing separation.

As shown in Figure 16c, the success rate of SSPPE-D is slightly higher than that of SSPPV-D. When the number of aircraft is 20, different weights result in varying success rates due to the domino effect of the first-come-first-served strategy. The differences between SSPPV-D and SSPPE-D in solution quality are overall not evident, but SSPPE-D is significantly slower than SSPPV-D, as shown in Figure 16d. For example, the runtime of SSPPE-D exceeds 1,400 ms for a weight of 0.8 and 20 aircraft in the absence of static obstacles, while SSPPV-D remains below 200 ms. The runtime at a weight of 1 deviates from the trend observed between 0 and 0.8. This may be because, without accounting for delay, the search process differs entirely from that of other weight settings.

7. Discussion

7.1. Comparison of conflict detection methods and algorithm variants

In this research, we propose three conflict detection methods for solution space generation. The distance-based method, closely associated with CPA, is widely used in the ATM field. The case study demonstrates that the distance-based method has the highest accuracy for conflict detection, with an average success rate of 99.67% in identifying near-optimal conflict-free paths when the grid size is 5 nmi and the number of rerouting points is limited to 5. However, this method is the slowest; under the same settings, the average runtime is approximately 12.53 ms for SSPPV-D and 49.75 ms for SSPPE-D. Since the distance-based method needs to compute the predicted minimum separation between a pair of aircraft, it may face computational challenges as the number of aircraft increases.

In contrast, the time-interval-based method, related to Safe Interval Path Planning (SIPP), is the most conservative approach and is very common in the path-planning field. This method maps and stores aircraft trajectories onto grids,

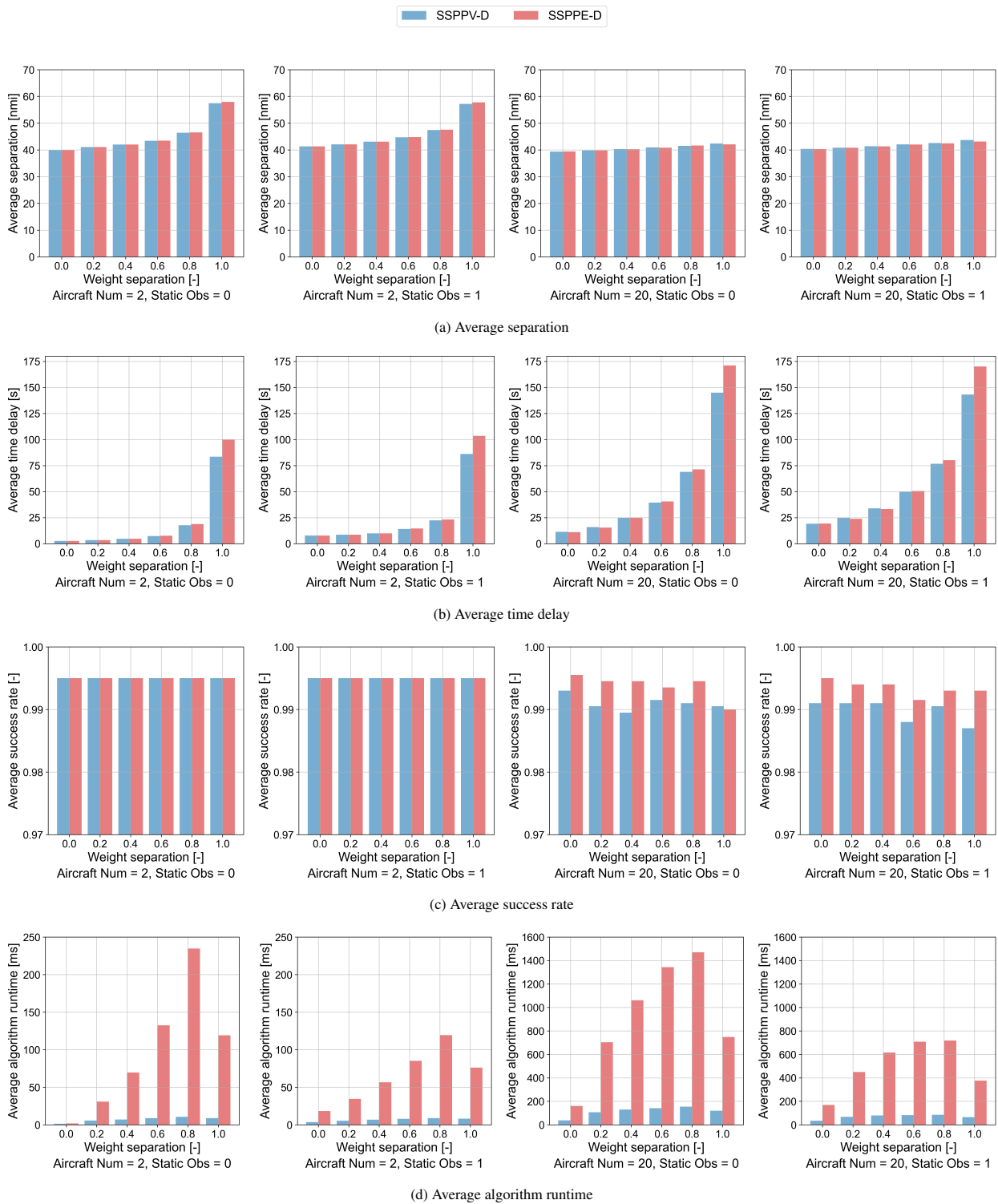


Figure 16: Algorithm results with fixed rerouting waypoints at 5 and grid size at 5 nmi, and varying weight settings.

making it particularly suitable for scenarios involving a large number of aircraft. It can also address dynamic obstacles with variable speeds, which can similarly be mapped as time intervals onto grids. However, this method is sensitive to grid size and may lead to lower success rates when the grid size is large. For example, when the grid size is 5 nmi and the number of rerouting points is limited to 5, the average success rate of the time-interval-based method is 91.58% and may drop to around 79.93% as the number of aircraft increases to 20.

The zone-based method, inspired by the Highly Interactive Problem Solver (HIPS), is tailored for solution space generation. The distance-based and time-interval-based methods function similarly to line-of-sight checks, whereas the zone-based method enables field-of-view generation for dynamic obstacles. The zone-based method demonstrates the fastest performance while maintaining a relatively high success rate (98.52%). The case study results show that it is 3.29 times faster than the distance-based method and 2.27 times faster than the time-interval-based method when the grid size is 5 nmi and the number of rerouting points is limited to 5. In this setup, the average runtime is approximately 3.69 ms for SSPPV-Z and 17.26 ms for SSPPE-Z. Another benefit of the zone-based method is that the conflict zones offer a clear visual explanation of where conflicts could arise and why certain nodes are unreachable, as shown in Figure 12. This is expected to improve the explainability and transparency of SSPP and may enhance the acceptance and trust of ATCos [4, 18].

Building upon the solution space and A* search, two different types of search nodes are proposed, which lead to the design of SSPPV and SSPPE. The case study results, to our surprise, indicate that SSPPV performs comparably to SSPPE in terms of delay and separation. Meanwhile, SSPPV is considerably faster than SSPPE. For example, when the grid size is 5 nmi and the number of rerouting waypoints is limited to 5, SSPPV is 3.77 times faster than SSPPE. This suggests that SSPPV is superior in most cases and particularly well-suited for tactical operations where time is constrained. In contrast, SSPPE may be more suitable for long-term strategic planning, where time is not an issue, due to its relatively higher success rates.

We also developed an extension of SSPP to optimize both delay and separation. The proposed extension is based on the distance-based conflict detection method, as this method calculates CPA values that can be used for optimization directly. The case study indicates that the proposed extension can substantially increase the separation between aircraft, particularly in scenarios with low traffic density. In practice, the ATC interface can be designed to allow ATCos to adjust the weight of the objective function to accommodate their individual preferences. Future research could explore how to implement multi-objective optimization based on zone-based conflict detection and consider additional objectives such as fuel consumption.

7.2. Limitations and future research

When designing algorithms for SSPP, we have three key assumptions. First, we focus on 2D rather than 3D path planning because the airspace is divided into flight levels, which decouples the altitude dimension from the horizontal dimension. Second, we assume a constant aircraft speed for path planning, as heading changes are generally preferred over speed changes for conflict resolution in en-route ATC. Third, we ignore aircraft turning dynamics and trajectory

uncertainties, which is a common assumption used to simplify the path-planning problem.

To extend the applicability of SSPP to more complex environments, these assumptions can be readily relaxed or compensated for. Relaxing the first two assumptions naturally introduces two additional conflict resolution mechanisms: altitude adjustments and speed adjustments. Therefore, we can define an ordered sequence of conflict resolution strategies: for example, first attempt heading changes; if that fails, adjust flight levels; and if conflicts still remain, modify speed. In this way, a three-layer solution space can be constructed. The first layer corresponds to the solution space considered in this article, where conflicts are resolved using only heading changes. The second layer focuses on cells that are unreachable in the first layer and attempts to make them reachable through altitude adjustments. The third layer addresses cells that remain unreachable after altitude adjustments by modifying speed. The remaining search procedures for path planning are the same. The approach described here is only one potential extension. Future research could examine in depth how to extend the solution space concept and solution space path planning to 3D, as well as how to incorporate speed adjustments.

The third assumption can be addressed by adding a buffer to the minimum separation standard. While this method may introduce additional delay, it is the simplest way to mitigate the issue. In practice, ATCos also deal with uncertainties by incorporating separation buffers in their decisions. When ATCos use SSPP as a decision-support tool, they should be aware of this assumption and continuously monitor aircraft trajectories to ensure safety. They may also be allowed to adjust the separation buffer as needed.

To further validate the effectiveness of SSPP and facilitate its real-world application, future research can conduct human-in-the-loop experiments to explore how ATCos collaborate and interact with SSPP in operations, and whether the solution space concept truly plays a role in their understanding, acceptance, and trust in path-planning algorithms. This involves not only algorithm design, but also the design of human-machine interaction and interfaces. The case study results highlight the importance of the order in conflict-free path planning (conflict resolution), which is also an interesting direction for future research.

8. Conclusion

This paper presents a Solution Space Path Planning (SSPP) algorithm for supporting en-route Air Traffic Control (ATC)—including multiple algorithmic variants—designed to balance interpretability, computational efficiency, operational compliance, and solution optimality. This algorithm combines the advantages of solution space and any-angle path planning, offering strong interpretability potential for human supervision along with straight and near-optimal paths for aircraft routing. To accelerate visibility checks involving static obstacles, shadowcasting has been integrated. For dynamic obstacles, three conflict detection methods have been introduced: distance-based, time-interval-based, and zone-based. When the grid size is 5 nmi, the distance-based method achieves a 99.67% success rate, with average runtimes of approximately 12.53 ms for SSPPV-D and 49.75 ms for SSPPE-D. The time-interval-based method has the lowest success rate (91.58%), which may drop to about 79.93% as the number of aircraft increases to 20.

The zone-based method is generally 3.29 times faster than the distance-based method and 2.27 times faster than the time-interval-based method, while still maintaining a relatively high success rate (98.52%).

Building on the solution space and A* search, we develop two SSPP variants: SSPPV and SSPPE. Overall, SSPPV achieves similar solution quality to SSPPE but offers about 3.77 times faster computation, making it more suitable for tactical operations. To enhance the robustness of path planning, an extension of SSPP has been proposed, with a focus on the trade-off between delay and separation. Given the interpretable structure of the solution space, the deterministic nature of the A*-based search, and its ability to generate operationally compliant routes, we believe that the proposed SSPP holds significant promise for advancing aviation automation in human-centric ways. Future research should investigate how operators interact with SSPP in operational settings through human-in-the-loop experiments.

Declaration of competing interest

The authors declare that they have no known competing financial interests or personal relationships that could have appeared to influence the work reported in this paper.

Acknowledgements

The authors would like to thank the financial support from the China Scholarship Council (CSC) No. 202106830036.

References

- [1] SESAR, Automation in Air Traffic Management, Technical Report, SESAR Joint Undertaking, 2020.
- [2] SESAR, European ATM master plan, Technical Report, SESAR Joint Undertaking, 2025. URL: <https://www.sesarju.eu/masterplan>.
- [3] EASA, Artificial Intelligence Roadmap 2.0: A human-centric approach to AI in aviation, Technical Report, European Union Aviation Safety Agency, 2023. URL: <https://www.easa.europa.eu/en/downloads/137919/en>.
- [4] Y. Zou, C. Borst, Investigating transparency needs for supervising unmanned air traffic management systems, in: 13th SESAR Innovation Days, 2023, pp. 1–9.
- [5] M. R. Endsley, Supporting human-AI teams: Transparency, explainability, and situation awareness, *Computers in Human Behavior* 140 (2023) 107574.
- [6] C. Westin, C. Borst, B. Hilburn, Strategic conformance: Overcoming acceptance issues of decision aiding automation?, *IEEE Transactions on Human-Machine Systems* 46 (2015) 41–52.
- [7] A. Barredo Arrieta, N. Díaz-Rodríguez, J. Del Ser, A. Bennetot, S. Tabik, A. Barbado, S. Garcia, S. Gil-Lopez, D. Molina, R. Benjamins, R. Chatila, F. Herrera, Explainable artificial intelligence (XAI): Concepts, taxonomies, opportunities and challenges toward responsible AI, *Information Fusion* 58 (2020) 82–115. doi:<https://doi.org/10.1016/j.inffus.2019.12.012>.
- [8] D. Gunning, D. Aha, DARPA's explainable artificial intelligence (XAI) program, *AI Magazine* 40 (2019) 44–58. doi:10.1609/aimag.v40i2.2850.
- [9] Y. Zou, C. Borst, Algorithmic transparency in path planning: A visual approach to enhancing human understanding, *International Journal of Human-Computer Studies* 203 (2025) 103573. doi:10.1016/j.ijhcs.2025.103573.
- [10] A. Bhat, A. Raychowdhury, Non-uniform interpolation in integrated gradients for low-latency explainable-ai, in: 2023 IEEE International Symposium on Circuits and Systems (ISCAS), IEEE, 2023, pp. 1–5.

- [11] J. Rasmussen, K. J. Vicente, Coping with human errors through system design: implications for ecological interface design, *International Journal of Man-machine Studies* 31 (1989) 517–534.
- [12] K. J. Vicente, J. Rasmussen, The ecology of human-machine systems ii: Mediating direct-perception in complex work domains, *Ecological Psychology* 2 (1990) 207–249.
- [13] K. J. Vicente, J. Rasmussen, Ecological interface design: Theoretical foundations, *IEEE Transactions on Systems, Man, and Cybernetics* 22 (1992) 589–606.
- [14] M. M. van Paassen, C. Borst, J. Ellerbroek, M. Mulder, J. M. Flach, Ecological interface design for vehicle locomotion control, *IEEE Transactions on Human-Machine Systems* 48 (2018) 541–555.
- [15] R. Klomp, R. Riegman, C. Borst, M. Mulder, M. Van Paassen, Solution space concept: Human-machine interface for 4D trajectory management, in: *Proceedings of the Thirteenth USA/Europe Air Traffic Management Research and Development Seminar (ATM2019)*, Vienna, Austria, 2019, pp. 17–21.
- [16] C. Borst, J. M. Flach, J. Ellerbroek, Beyond ecological interface design: Lessons from concerns and misconceptions, *IEEE Transactions on Human-Machine Systems* 45 (2015) 164–175. doi:10.1109/THMS.2014.2364984.
- [17] M. Mulder, C. Borst, M. M. van Paassen, Improving operator situation awareness through ecological interfaces: Lessons from aviation, in: *1st International Conference on Computer-Human Interaction Research and Applications, CHIRA 2017*, Springer, 2019, pp. 20–44.
- [18] C. Westin, C. Borst, E. Kampen, T. M. Nunes, S. Boonsong, B. Hilburn, M. Cocchioni, S. Bonelli, Personalized and transparent AI support for ATC conflict detection and resolution: an empirical study, *Proceedings of the 12th SESAR Innovation Days*, Budapest, Hungary (2022) 5–8.
- [19] W. Dai, B. Pang, K. H. Low, Conflict-free four-dimensional path planning for urban air mobility considering airspace occupancy, *Aerospace Science and Technology* 119 (2021) 107154.
- [20] Y. Chen, M. Hu, L. Yang, Autonomous planning of optimal four-dimensional trajectory for real-time en-route airspace operation with solution space visualisation, *Transportation Research Part C: Emerging Technologies* 140 (2022) 103701.
- [21] Y. Chen, Y. Xu, L. Yang, M. Hu, In-flight fast conflict-free trajectory re-planning considering UAV position uncertainty and energy consumption, *Transportation Research Part C: Emerging Technologies* 171 (2025) 104988.
- [22] B. Bergström, FOV using recursive shadowcasting, http://www.roguebasin.com/index.php?title=FOV_using_recursive_shadowcasting, 2001. Accessed on Aug. 2nd, 2025.
- [23] A. Milazzo, Roguelike vision algorithms, https://www.adammil.net/blog/v125_Roguelike_Vision_Algorithms.html, 2014. Accessed on Aug. 2nd, 2025.
- [24] K. Daniel, A. Nash, S. Koenig, A. Felner, Theta*: Any-angle path planning on grids, *J. Artif. Int. Res.* 39 (2010) 533–579.
- [25] K. Yakovlev, A. Andreychuk, Towards time-optimal any-angle path planning with dynamic obstacles, in: *Proceedings of the International Conference on Automated Planning and Scheduling*, volume 31, 2021, pp. 405–414.
- [26] P. E. Hart, N. J. Nilsson, B. Raphael, A formal basis for the heuristic determination of minimum cost paths, *IEEE Transactions on Systems Science and Cybernetics* 4 (1968) 100–107. doi:10.1109/TSSC.1968.300136.
- [27] M. Davoodi, Bi-objective path planning using deterministic algorithms, *Robotics and Autonomous Systems* 93 (2017) 105–115.
- [28] D. T. Öztürk, M. Köksalan, Biobjective route planning of an unmanned air vehicle in continuous space, *Transportation Research Part B: Methodological* 168 (2023) 151–169.
- [29] EUROCONTROL, LORD adds speed and flexibility to decisions for Maastricht controllers, *Skyway* (2024) 54–56. URL: <https://www.eurocontrol.int/article/lord-adds-speed-and-flexibility-decisions-maastricht-controllers>, accessed on Jun. 18th, 2025.
- [30] W. Lyu, C. Borst, M. R. van Paassen, M. Mulder, How do visualization choices affect human decision-making? a case study in air traffic control, in: *2025 IEEE International Conference on Systems, Man, and Cybernetics (SMC)*, IEEE, 2025, pp. 7109–7114. doi:10.1109/SMC58881.2025.11343058.
- [31] P. Fiorini, Z. Shiller, Motion planning in dynamic environments using velocity obstacles, *The International Journal of Robotics Research* 17

- (1998) 760–772. doi:10.1177/027836499801700706.
- [32] D. Wilkie, J. Van Den Berg, D. Manocha, Generalized velocity obstacles, in: 2009 IEEE/RSJ International Conference on Intelligent Robots and Systems, IEEE, 2009, pp. 5573–5578.
- [33] F. Vesentini, R. Muradore, P. Fiorini, A survey on velocity obstacle paradigm, *Robotics and Autonomous Systems* 174 (2024) 104645.
- [34] G. A. M. Velasco, C. Borst, M. M. van Paassen, M. Mulder, Solution space decision support for reducing controller workload in route merging task, *Journal of Aircraft* 58 (2021) 125–137. doi:10.2514/1.C035852.
- [35] C. Borst, R. M. Visser, M. M. van Paassen, M. Mulder, Exploring short-term training effects of ecological interfaces: A case study in air traffic control, *IEEE Transactions on Human-Machine Systems* 49 (2019) 623–632. doi:10.1109/THMS.2019.2919742.
- [36] C. Borst, V. A. Bijsterbosch, M. M. van Paassen, M. Mulder, Ecological interface design: supporting fault diagnosis of automated advice in a supervisory air traffic control task, *Cognition, Technology & Work* 19 (2017) 545–560. doi:10.1007/s10111-017-0438-y.
- [37] C. Meckiff, P. Gibbs, Phare highly interactive problem solver, *EEC Re* (1994).
- [38] B. J. van Marwijk, C. Borst, M. Mulder, M. Mulder, M. M. van Paassen, Supporting 4D trajectory revisions on the flight deck: Design of a human-machine interface, *The International Journal of Aviation Psychology* 21 (2011) 35–61.
- [39] M. Van Paassen, C. Borst, R. Klomp, M. Mulder, P. van Leeuwen, M. Mooij, Designing for shared cognition in air traffic management, *Journal of Aerospace Operations* 2 (2013) 39–51.
- [40] R. Klomp, C. Borst, R. van Paassen, M. Mulder, Expertise level, control strategies, and robustness in future air traffic control decision aiding, *IEEE Transactions on Human-Machine Systems* 46 (2015) 255–266.
- [41] S. B. Van Dam, M. Mulder, M. Van Paassen, Ecological interface design of a tactical airborne separation assistance tool, *IEEE Transactions on Systems, Man, and Cybernetics-Part A: Systems and Humans* 38 (2008) 1221–1233.
- [42] SESAR, AI in ATM: transparency, explainability, conformance, situation awareness and trust, Technical Report, SESAR Joint Undertaking, 2022. URL: <http://mahaloproject.eu/wp-content/uploads/2022/12/Sesar-white-paper.pdf>.
- [43] R. Siegwart, I. R. Nourbakhsh, D. Scaramuzza, *Introduction to autonomous mobile robots*, MIT press, 2011.
- [44] B. Shen, M. A. Cheema, D. D. Harabor, P. J. Stuckey, Fast optimal and bounded suboptimal euclidean pathfinding, *Artificial Intelligence* 302 (2022) 103624.
- [45] J. Li, C. Yu, Z. Zhang, Z. Sheng, Z. Yan, X. Wu, W. Zhou, Y. Xie, J. Huang, Improved a-star path planning algorithm in obstacle avoidance for the fixed-wing aircraft, *Electronics* 12 (2023) 5047.
- [46] A. Almozel, E. M. Feron, S. I. Saber, C. Cloiseau, K. Vanderventer, Safe trajectory planning for safety critical drone delivery, in: *AIAA Aviation 2023 Forum*, 2023, p. 3547.
- [47] P. Yap, N. Burch, R. Holte, J. Schaeffer, Block A*: Database-driven search with applications in any-angle path-planning, *Proceedings of the AAAI Conference on Artificial Intelligence* 25 (2011) 120–125. doi:10.1609/aaai.v25i1.7813.
- [48] D. Harabor, A. Grastien, D. Öz, V. Aksakalli, Optimal any-angle pathfinding in practice, *J. Artif. Int. Res.* 56 (2016) 89–118.
- [49] N. Rivera, C. Hernández, N. Hormazábal, J. A. Baier, The 2^k neighborhoods for grid path planning, *Journal of Artificial Intelligence Research* 67 (2020) 81–113.
- [50] S. R. Bassolillo, G. Raspaolo, L. Blasi, E. D’Amato, I. Notaro, Path planning for fixed-wing unmanned aerial vehicles: An integrated approach with theta* and clothoids, *Drones* 8 (2024) 62.
- [51] D. Silver, Cooperative pathfinding, *Proceedings of the AAAI Conference on Artificial Intelligence and Interactive Digital Entertainment* 1 (2005) 117–122. doi:10.1609/aiide.v1i1.18726.
- [52] A. Vemula, K. Muelling, J. Oh, Path planning in dynamic environments with adaptive dimensionality, in: *Proceedings of the International Symposium on Combinatorial Search*, volume 7, 2016, pp. 107–115.
- [53] M. Phillips, M. Likhachev, SIPP: Safe interval path planning for dynamic environments, in: 2011 IEEE International Conference on Robotics and Automation, IEEE, 2011, pp. 5628–5635.
- [54] M. von der Burg, A. Sharpanskykh, Multi-agent planning for autonomous airport surface movement operations, *SESAR Innovation Days 2023* (2023).

- [55] K. Yakovlev, A. Andreychuk, Any-angle pathfinding for multiple agents based on SIPP algorithm, in: Proceedings of the International Conference on Automated Planning and Scheduling, volume 27, 2017, pp. 586–594.
- [56] Y. Zou, C. Borst, Zeta*-SIPP: Improved time-optimal any-angle safe-interval path planning, in: Proceedings of the 33rd International Joint Conference on Artificial Intelligence, 2024, pp. 6823–6830. doi:10.24963/ijcai.2024/754.
- [57] A. Andreychuk, K. Yakovlev, P. Surynek, D. Atzmon, R. Stern, Multi-agent pathfinding with continuous time, *Artificial Intelligence* 305 (2022) 103662.
- [58] K. Yakovlev, A. Andreychuk, R. Stern, Optimal and bounded suboptimal any-angle multi-agent pathfinding, in: 2024 IEEE/RSJ International Conference on Intelligent Robots and Systems (IROS), IEEE, 2024, pp. 7996–8001.
- [59] G. Sharon, R. Stern, A. Felner, N. R. Sturtevant, Conflict-based search for optimal multi-agent pathfinding, *Artificial Intelligence* 219 (2015) 40–66.
- [60] J. Wang, W. Chi, C. Li, C. Wang, M. Q.-H. Meng, Neural RRT*: Learning-based optimal path planning, *IEEE Transactions on Automation Science and Engineering* 17 (2020) 1748–1758.
- [61] D. Kirilenko, A. Andreychuk, A. I. Panov, K. Yakovlev, Generative models for grid-based and image-based pathfinding, *Artificial Intelligence* 338 (2025) 104238.
- [62] EASA, Machine learning application approval, <https://www.easa.europa.eu/en/research-projects/machine-learning-application-approval>, 2024. Accessed on Jul. 2nd, 2025.
- [63] M. Herman, Towards Explainable Automation for Air Traffic Control Using Deep Q-learning from Demonstrations and Reward Decomposition, Master’s thesis, Delft University of Technology, Faculty of Aerospace Engineering, 2021.
- [64] Z. Juozapaitis, A. Koul, A. Fern, M. Erwig, F. Doshi-Velez, Explainable reinforcement learning via reward decomposition, in: IJCAI/ECAI Workshop on Explainable Artificial Intelligence, 2019.
- [65] G. Papadopoulos, A. Bastas, G. A. Vouros, I. Crook, N. Andrienko, G. Andrienko, J. M. Cordero, Deep reinforcement learning in service of air traffic controllers to resolve tactical conflicts, *Expert Systems with Applications* 236 (2024) 121234.
- [66] Y. Zou, C. Borst, Towards a unified taxonomy for algorithmic transparency: insights from uncrewed air traffic management, *Cognition, Technology & Work* 28 (2026) 229–255.
- [67] S. Manzinger, C. Pek, M. Althoff, Using reachable sets for trajectory planning of automated vehicles, *IEEE Transactions on Intelligent Vehicles* 6 (2020) 232–248.
- [68] J. E. Bresenham, Algorithm for computer control of a digital plotter, in: *Seminal graphics: pioneering efforts that shaped the field*, 1998, pp. 1–6.
- [69] X. Wu, An efficient antialiasing technique, *ACM Siggraph Computer Graphics* 25 (1991) 143–152.
- [70] Y. Zou, H. Zhang, G. Zhong, H. Liu, D. Feng, Collision probability estimation for small unmanned aircraft systems, *Reliability Engineering & System Safety* 213 (2021) 107619.
- [71] M. Jardin, Grid-based strategic air traffic conflict detection, in: *AIAA Guidance, Navigation, and Control Conference and Exhibit*, 2005, p. 5826.
- [72] J. Koeners, M. de Vries, Conflict resolution support for air traffic control based on solution spaces: Design and implementation, in: 2008 IEEE/AIAA 27th Digital Avionics Systems Conference, IEEE, 2008, pp. 3–C.
- [73] G. A. M. Velasco, C. Borst, J. Ellerbroek, M. Van Paassen, M. Mulder, The use of intent information in conflict detection and resolution models based on dynamic velocity obstacles, *IEEE Transactions on Intelligent Transportation Systems* 16 (2015) 2297–2302.
- [74] H. Idris, R. Vivona, J.-L. Garcia-Chico, D. Wing, Distributed traffic complexity management by preserving trajectory flexibility, in: 2007 IEEE/AIAA 26th Digital Avionics Systems Conference, IEEE, 2007, pp. 3–B.
- [75] H. Idris, T. El-Wakil, D. Wing, Trajectory planning by preserving flexibility: metrics and analysis, in: *AIAA Guidance, Navigation and Control Conference and Exhibit*, 2008, p. 7406.
- [76] R. Whelan, Effective analysis of reaction time data, *The Psychological Record* 58 (2008) 475–482.